May 2024

Polycrystalline catalysis studied with time-resolved ambient pressure x-ray photoelectron spectroscopy

Julia Prumbs

Project duration: 9 months, 60 ECTS

Thesis submitted for degree Master of Science
Supervised by Jan Knudsen

LUND
UNIVERSITY

Department of Physics
Division of Synchrotron Radiation Research

Abstract

Polycrystals, crystals consisting of multiple grains with different crystallographic orientations, gained interest in recent years as they mimic industrial catalysts. They have been studied thoroughly utilizing imaging techniques to investigate the various surface structures of the grains; however, measurements under ambient pressure conditions are necessary for closing the pressure gap. In this thesis, I demonstrate that ambient pressure x-ray photoelectron spectroscopy can be used for not only measuring the surface but also the corresponding gas phase for each grain individual using CO oxidation as a test reaction. To study how the surface structure and the observed catalytic activity are connected, time-resolved measurements are performed. To stimulate surface structural changes of the used Pd catalyst the temperature is oscillated periodically. Using Fourier-transformed experiments I selectively detect/probe the temperature-induced changes at the surface of the grains and in the gas phase above them. For instance, evidence for temperature-dependent opening of small vacancies in a primarily CO-covered surface was detected. By increasing the temperature oscillations to drive the catalyst into and out of the CO mass transfer limit, differences in the adsorption of CO to the surface in dependence on the crystallographic orientation could be proven, showing that Pd(111) is more prone to CO poisoning than Pd(100) and Pd(110).

Acronyms

AES	Auger Electron Spectroscopy
AP	Ambient Pressure
APXPS	Ambient Pressure X-ray Photoelectron Spectroscopy
CO-MTL	CO Mass Transfer Limit
EBSD	Electron BackScatter Diffraction
EPU	Elliptically Polarizing Undulator
FT	Fourier Transform
HAXPES	HArd X-ray PhotoElectron Spectroscopy
IFT	Inverse Fourier Transform
IFT image plot	Inverse Fourier transformed image plot without 0 Hz component
LEED	Low Energy Electron Diffraction
MES	Modulation Excitation Spectroscopy
MTL	Mass Transfer Limit
XPS	X-ray Photoelectron Spectroscopy
UHV	Ultra-High Vacuum
UPS	Ultraviolet Photoelectron Spectroscopy

Contents

1 Introduction

Catalysts are indispensable in today's industry and are used in numerous areas. An important and well-known application is in cars, where 3-way catalysts are used to convert H_xC_y, CO, and NO_x contained in the exhaust gases into less harmful substances [1]. Even the production of car fuels, which is done by the so-called hydrocracking, requires catalysts to convert crude oil to higher-value products such as gasoline or diesel [2,3]. Also important is the removal of sulfur from these fuels to avoid acid rain which also is done with catalysts [4]. However, catalysts are not only used in the oil and car industry. They are also indispensable in agriculture. Most of today's fertilizer is, for example, produced with the Haber-Bosch process, which utilizes a catalyst to produce ammonia from nitrogen and hydrogen [5].

With global warming as one of the largest problems for mankind, the switch to renewable energy sources is becoming increasingly important and is being actively promoted. However, such renewable energy sources are often very dependent on weather, time, and location. This is incompatible with our continuous energy demand anytime and everywhere. It is, therefore, very important to find efficient ways to store and transport energy in large quantities. Hydrogen generated by electrolysis or photocatalysis from renewable sources is often being brought into the spotlight as a large-scale storage option [6–8]. Furthermore, hydrogen is an appealing alternative to fossil fuels as water is the only exhaust product, making it a clean fuel that can be used in a fuel cell or combustion engine [9]. One downside of hydrogen is that it is very explosive. Therefore, it is not suitable for transportation over long distances or for storage in very large quantities. Most current plans to ensure safe and easy storage and transport of energy call for the conversion of hydrogen into ammonia, which requires catalysts as mentioned before [10]. Other plans include the use of methane or dimethyl ether, which again requires catalysts to convert them back to hydrogen, for example via methane steam reforming [10, 11]. New superior catalysts are therefore also indispensable for the future energy transition.

Most of the catalysts we know and use today have been developed by simple trial and error type experiments. With a fundamental knowledge of catalytic processes of known catalyst materials, it would become possible to design new superior catalysts without going through expensive screening experiments [12]. Such fundamental knowledge is unfortunately difficult to obtain by studying real catalysts as they are composed of many different materials and for this reason, so-called ultra-high vacuum (UHV) experiments of highly simplified systems have been popular [13]. One main reason is that many surface-sensitive techniques only work in UHV, like x-ray photoelectron spectroscopy (XPS) [14], auger electron spectroscopy (AES) [15] or low energy electron diffraction (LEED) [16]. Secondly, experiments at controlled UHV conditions enable the maintenance of a clean sample surface making the characterization easier. Even though UHV studies have given us a lot of knowledge about gas adsorption, dissociation, and reactions on surfaces [15], they also have their limitations. Partial pressures can, for example, heavily affect the structure of the catalyst as well as the reaction kinetics and so consequently also the catalytic activity [17, 18]. Therefore, the use of data acquired in UHV conditions can only partly be applied to real catalysts. The gap in knowledge between the detailed understanding of adsorption, dissociation, diffusion,

and reactions at UHV conditions and our limited knowledge about catalysts at more realistic pressure is often referred to as a pressure gap [15, 19]. To gain knowledge about the structure-function relationship of catalyst surfaces in situ measurements are needed [19]. To enable these in situ measurements different techniques have been developed. One of these techniques is ambient pressure x-ray photoelectron spectroscopy (APXPS) [20]. One advantage of this technique is that it allows us to measure not only the catalyst's surface structure but also the gas phase in the near vicinity of the surface. Consequently, a direct correlation can be made between the gas composition above the surface and the catalytic activity of the surface structure.

Many previous catalyst studies used single crystals, but this is far from the reality of catalysts used in industry. Industrial catalysts usually consist of small metal particles with a size of about 1 to 10 nm on a support material [21]. These catalysts have a lot of different facets with different crystallographic orientations and following different surface structures. The difference between the highly simplified single crystal surface and the many different facets on real catalyst particles is often called a material gap. One way to preserve the control and easy interpretation that single crystal surfaces offer and at the same time partly overcome the material gap is to use so-called polycrystals. These crystals consist of multiple grains with different crystallographic orientations [22, 23].

In the past, catalysts have been studied mostly under static conditions, meaning constant pressure, temperature, and gas composition, when they are catalytic active. This approach gives information about which structure is covering the catalyst surface when the catalyst is active. However, it does not allow us to determine if the detected majority structure is actually catalytic active or if there is a minority structure, which causes the catalytic activity. To answer this question time-resolved measurements are necessary [24]. Hereby, it becomes possible to determine how changes in the catalyst surface structure are correlated to the catalytic activity as well as to determine if there are any catalytic active transient structures. Examples of, time-resolved catalysis methods include surface-sensitive time-resolved infrared spectroscopy [25], time-resolved in situ Raman spectroscopies [26] or time-resolved APXPS [24, 27].

When studying surface structure changes between different states the probed signal can be dominated by atoms and/or molecules of the catalyst that are static and spectators for the catalytic process. In the case of APXPS, it is caused by either the measured bulk atoms or the static surface components, which makes it difficult to identify the much smaller changing components. One way to improve the resolution of the experiment is the concept of modulation excitation spectroscopy (MES) [28]. When applying this idea to APXPS, the basic idea is to modulate the system by periodically changing external parameters like the temperature, the pressure, or the gas composition. This leads to a change in surface coverage, which can be detected by the electron analyser. In this case, the oscillating external parameters equal the "excitation". Within this method typically multiple periods are averaged to improve the signal-to-noise ratio [24]. A newly developed method by Knudsen is based on this idea, but instead of event averaging the data, Fourier transformations (FT) are utilized to selectively probe the changing components [29]. I used this method in my thesis

by applying temperature oscillations periodically, resulting in an oscillating surface coverage.

The main goal of my thesis has been to investigate if it is possible to selectively probe and correlate surface structure changes with changes in the catalytic activity on polycrystal surfaces. The individual grains of the used Pd crystal were around 0.5 mm $\times$ 0.5 mm each. The various crystallographic orientations of the different grains were determined in a previous study using electron backscatter diffraction (EBSD) [30]. As a test reaction CO oxidation was chosen, since it is well-studied for Pd catalysts under static conditions [31–33]. The knowledge of the expected surface coverage for different crystallographic orientations makes it possible to directly prove if it is possible to measure the grains individually using APXPS. The measurement of the individual grains makes it possible to directly compare the catalytic activity of different crystallographic orientations under the exact same surrounding conditions.

For this thesis two different datasets from our synchrotron measurements on a Pd polycrystal will be analysed and discussed: The first dataset was recorded while oscillating the polycrystal temperature within a range ensuring that the surface was mainly CO-covered and having low activity. The goal of this experiment was to answer whether it is possible to observe different catalytic activities of the different grains while in the CO-poisoned state. The second dataset was recorded with larger temperature oscillations to drive the catalyst into and out of the CO mass transfer limit (MTL), meaning that all CO from the gas phase is combusted. For all data analysis, Fourier transformation will be utilized to observe the changes between the different states, as described before.

I started my thesis in August 2023, but since the beamtime for the Pd polycrystal was first in November 2023, the data analysis is explained using a previously measured dataset. In this dataset, a single Pt(111) crystal was studied, while driving it into and out of the mass transfer limit using temperature oscillation. Although the dataset was originally only intended as an illustrative example to explain the data analysis, it revealed some interesting information about the transition between a CO-covered and O-covered surface.

2 Theory

2.1 Heterogenous catalysis

Heterogenous catalysis describes catalytic processes in which reactants/products are in a different phase than the catalyst material [34]. The advantage of heterogeneous catalysis, especially for industrial use, is that the different phases make it easy to separate the products from the catalyst. In the case of this study, the reactants and products are gaseous while the catalyst is solid. When the gas atoms/molecules form a chemical bond with the surface the intermolecular bonds can be weakened as electron density is used to form the molecule-surface bond [35]. This consequently leaves very active molecules behind, that can react with other atoms that are also adsorbed to the surface. This process is employed for heterogeneous catalysts. The interaction of the chemisorbed gases is extremely substance-

dependent. While for example O_2 dissociates and leaves active O atoms on the Pd surface behind, other molecules like CO do not dissociate [36]. For CO oxidation, these active oxygen atoms on the surface react with the also adsorbed CO molecules to form CO_2 and then desorb from the surface, see Figure 1 (a). This catalytic process significantly reduces the activation energy needed for a reaction, see Figure 1 (b). If not enough energy is provided for the catalytic reaction or not enough O_2 is in the gas phase, adsorbed CO can occupy the whole surface, since it does not dissociate. The catalyst is then called CO poisoned [35].

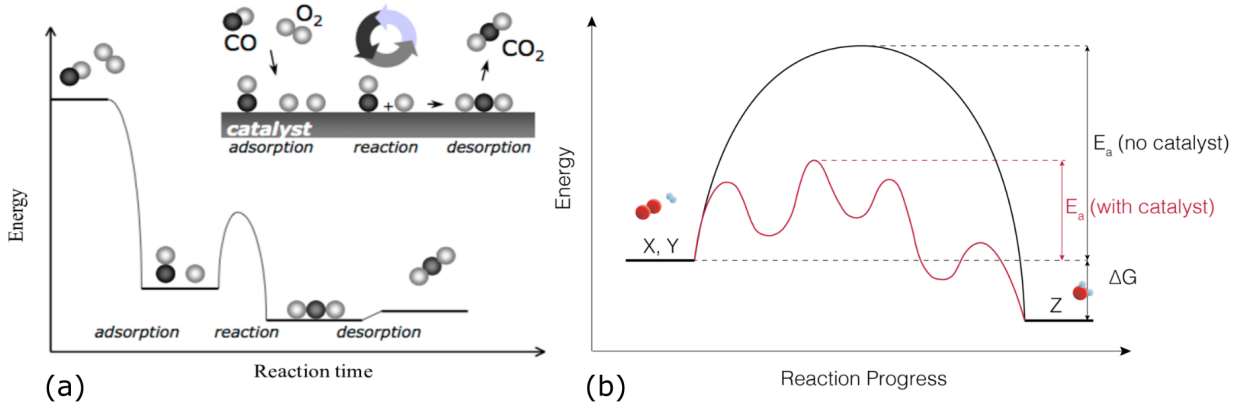

Figure 1: **Schematic energy diagram and reaction cycle for catalytic reaction**, (a) CO oxidation schematic reaction cycle. The figure is taken from [37]. (b) Schematic energy diagram for Reaction with and without catalyst. The figure is taken from [38].

2.2 Ambient pressure x-ray photoelectron spectroscopy

To understand solid heterogeneous catalysts, it is essential to study the surface structure of the catalysts. One common surface analysis technique is x-ray photoelectron spectroscopy. One benefit of XPS is that it makes it possible to determine atomic composition and surface chemistry through the so-called chemical shift simultaneously.

The basic working principle of XPS is that an x-ray beam is used to irradiate the studied surface. If the energy of the incoming photons is high enough, electrons are ejected from the atoms. These ejected electrons have a kinetic energy of

$$E_{kin} = h\nu - E_{Bin}, \tag{1}$$

here E_{kin} is the kinetic energy of the ejected electron and E_{Bin} is the binding energy of the electron [14]. The work function shifts will be neglected for now and explained in a later chapter. The kinetic energy of the ejected photoelectrons is measured using an electron analyser. It is especially interesting to study the core-level electrons since their binding energy is element-specific. Together with tabulated cross sections (the probability to generate an electron by a photon [39]), this makes it possible to not only study which elements are adsorbed to the surface but also the ratio they appear relative to each other. Another important fact is that the core-level binding energy is influenced by the chemical state of the atom.

For example, when oxygen bonds to a Pd surface, the Pd atom's electrons shift toward the oxygen due to the difference in electronegativity, creating a partial positive charge on Pd and a partial negative charge on oxygen [40]. This causes a shift in the binding energy of core-level electrons, the so-called chemical shift, which can be measured.

For the study of catalysis, it is of course very interesting to see how the catalyst surface changes depending on the gas phase. The problem with XPS is that it is typically done in ultra-high vacuum conditions. Since the kinetic energy of the electrons is used to determine the binding energy of the electrons, see Equation 1, only elastic scattered electrons contribute to the observed peaks in the spectra. All electrons that are scattered inelastically, meaning that they lose energy, become part of the background. To maximize the surface sensitivity, typically a photon energy is chosen that is only 80 to 120 eV larger than the binding energy of the core-level electrons. These low-energy electrons have a high cross-section. To describe how far an electron can travel before it scatters inelastically in a gas or solid the electron attenuation length is used. In the gas phase, electron attenuation (AL) is proportional to $e^{\frac{\sigma dp}{kT}}$ [41], where σ refers to the cross-section, d to the distance, p to the pressure, k to the Boltzmann constant and T to the temperature. The equation $AL \propto e^{\frac{\sigma dp}{kT}}$ shows that the electron attenuation increases exponentially with the pressure as well as with the cross-section. The high cross-section of the electrons leads to that even at low pressures the electrons can only travel a short distance before so many of them are inelastically scattered that the signal-to-noise ratio of the measurement is very bad. For example, at a pressure of one mbar the electron attenuation length would only be around one millimeter. [41]

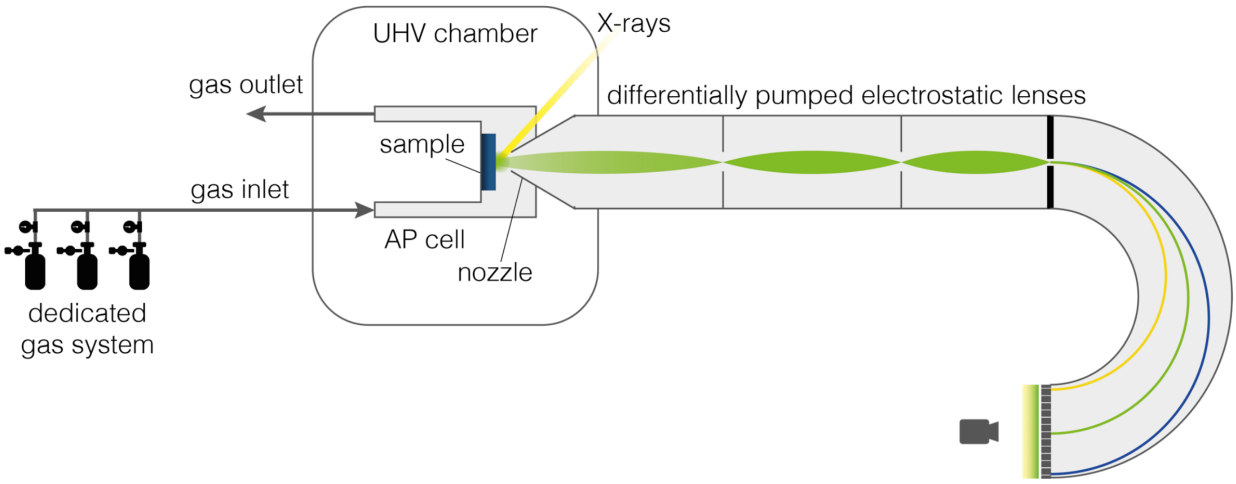

Figure 2: Schematic illustration of the ambient pressure - XPS setup at Hippie. The figure is taken from [38].

A closer look at the equation also shows that the electron attenuation is also exponentially increasing with the distance d that the electron needs to travel in the gas phase. Since the cross-section cannot be changed and the pressure will be increased, the distance must be decreased. This can be achieved by using a system of sequential pumping chambers, see

Figure 2. Each used pumping chamber has a lower pressure than the previous one. With such a setup the electron attenuation length can be substantially prolonged. One problem is that through the different chambers, the detection solid angle of the electrons is decreased. To fix this, electrostatic lenses are used to bundle the electrons and thus increase the amount of detected electrons. Using a combination of these two principles it is possible to reach an acceptance angle of electrons that is close to classical XPS in vacuum. [14] Using the principle of differential pumping pressures close to ambient pressure can be reached. For example, the HIPPIE beamline, which is used for the experiment in this thesis, can reach pressures up to 30 mbar [42]. For my thesis a pressure of around 1 mbar was used, this has the advantage that the observed gas and surface peaks have a comparable intensity relative to each other, making it possible to also see gas phase peaks in the spectra when measuring the surface.

3 Measuring set up

All measurements were taken at the A-branch of the HIPPIE endstation at MAX IV. The HIPPIE beamline is located at the 3 GeV storage ring, making it possible to reach a high photon flux of over 10^{12} s^{-1} at a large energy range of 250 to 2200 eV. The end station's instrumentation enables a resolving power of more than 10000 for energies ranging from 250 to 2000 eV. The used x-rays for the end station are created by an elliptically polarizing undulator (EPU). I will not further discuss the optical design of the beamline, more information about it can be found in [42].

3.1 HIPPIE

The whole set-up of the HIPPIE endstation can be seen in Figure 3. Additionally to the analysis chamber, the endstation is equipped with a UHV preparation chamber, a load lock chamber, and a radial distribution chamber which makes it easy to move the samples between the different components. For this experiment, the catalyst was mounted on a stainless steel sample plate equipped with a type K thermocouple, that enabled the measurement of the temperature of the sample. The gas-dosing system in the preparation chamber was used to sputter the crystal with Argon and the installed e-beam heater to anneal the sample subsequently. Using the radial distribution chamber the sample was moved to the analysis chamber, which can be seen on the top right side of Figure 3. The analysis chamber is connected with a ScientaOmicron HiPP-3 electron analyser, which uses differential pumping stages as well as electrostatic lenses to enable measurements under pressure of up to 30mbar. [42] For this experiment a time resolution of 120 ms was reached.

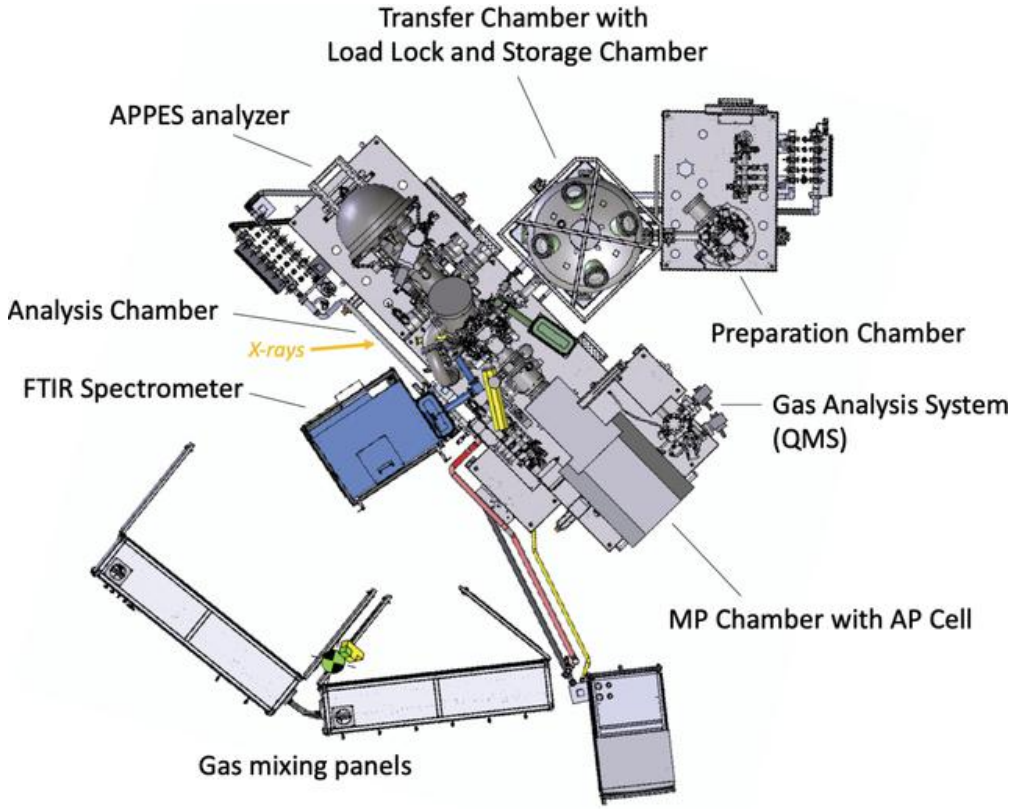

Figure 3: **Set-up of HIPPIE end station** The figure is taken from [42].

3.2 Ambient Pressure XPS cell

For my catalysis measurements a cell-in-cell approach [41] was used. In this approach, an additional high-pressure chamber is installed inside the analysis chamber. This cell can be directly docked to the electron analyser, making it possible to only fill this cell with gases up to a pressure of 5 mbar, while keeping the rest of the analysis chamber at a pressure in the 10^{-7} mbar range. The ambient pressure (AP) cell is equipped with an x-ray window allowing the photons to enter the cell. When not in use the cell can be retracted and stored in the AP cell chamber to enable to do UHV measurements in the analysis chamber, without needing to bake. [42]

Within the AP cell, the sample can be moved sideways. Since catalysts typically become active at high temperatures it is necessary to heat the sample. This is done by using a fibre-coupled IR laser which heats the sample from the back using a wavelength of 800 nm. This makes it possible to heat the sample to a temperature up to 600 °C. [42]

Separate gas lines for the different gases with individual mass flow controllers, allow for direct regulation of the dosed gas composition into the cell as well as to change the used gases without needing to bake out the gas lines. The combination of the small cell volume of one liter and the use of two pumping lines, make it possible to fastly change the gas in the cell. An in-vacuum Pirani gauge, supported by a capacitance gauge and a full-range

gauge is used to monitor the pressure in the AP cell. A quadrupole mass spectrometer can be directly connected to the nozzle, the inlet, or the outlet lines of the cell, enabling one to directly see the change in gas composition upon exposure to the sample. [42]

3.3 Measuring positions

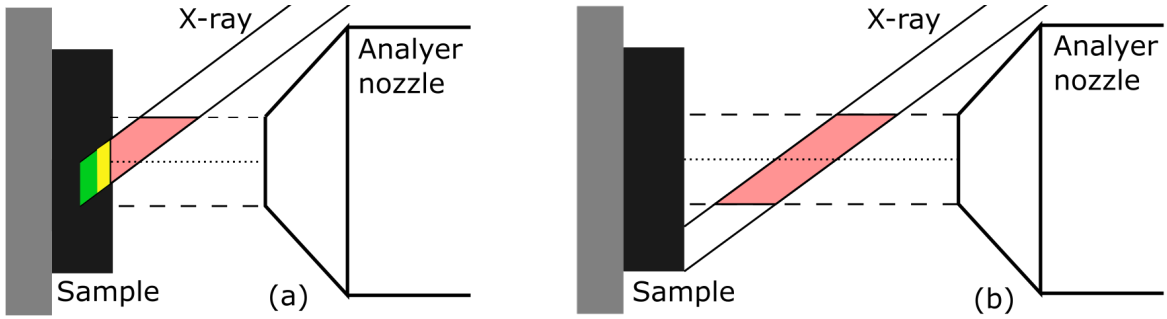

Figure 4: **Measuring positions of the analyser nozzle for (a) Surface measurements and (b) Gas phase measurements** red: measured gas phase, yellow: measured surface, green: measured bulk

Two different analyser positions were used to measure the gas and the surface spectra, respectively, see Figure 4. To measure the surface spectra (Figure 4 (a)) the analyser is placed closer to the sample. The photon energy for surface experiments is chosen such that the photoelectron has an energy at the order of 100 eV giving a mean free path of only a few atomic layers. As a result, the large majority of the signal originates from the topmost layers of the surface, which are illustrated in yellow in Figure 4 (a). Electrons generated by photons deeper in the bulk, shown in green in Figure 4 (a), lose kinetic energy when leaving the material. These electrons are called secondary electrons and are responsible for the background of the surface measurements. Since the experiments are carried out in ambient pressure, part of the gas phase is always detected as well, as shown by the red area in Figure 4 (a). To reach a similar magnitude both in the surface and gas phase spectra a pressure of approximately 1 mbar is typically used.

To measure the gas phase the sample is retracted, so that the point where the photon beam hits the surface is outside the focus of the electron analyser. As shown in Figure 4 (b) now mainly the gas phase is getting probed and only very few secondary electrons are measured.

3.4 Energy calibration

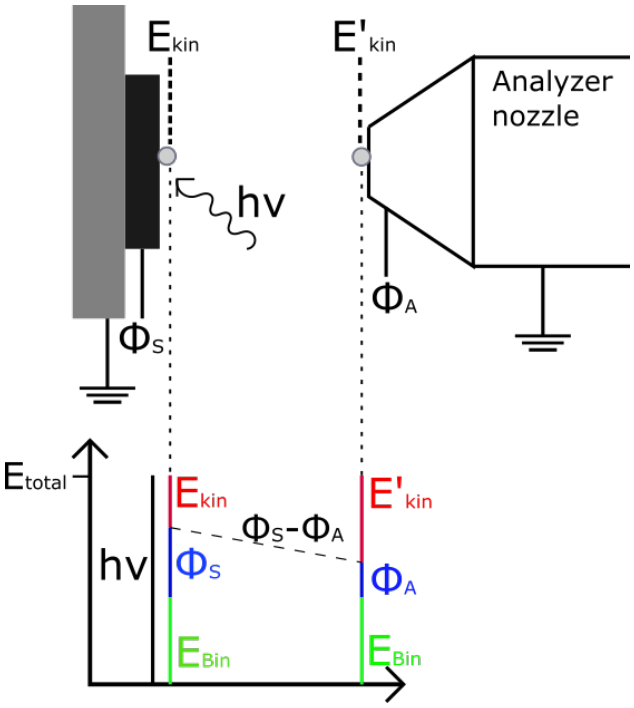

Figure 5: **Energy calibration**

The kinetic energy of an ejected electron from the surface of the catalyst depends on the energy of the incoming photon $h\nu$, the binding energy E_{Bin} of the electron, and the work function of the surface Φ_S [14].

$$E_{kin} = h\nu - E_{Bin} - \Phi_S \tag{2}$$

Now when the electron moves from the surface to the electron analyser, the work function of the electron analyser Φ_A needs to be considered as well. The electron is moving through the potential $\Phi_S - \Phi_A$, see Figure 5. Assuming $\Phi_S > \Phi_A$, the kinetic energy of the electron is increasing. In general, when the electron reaches the analyser, the kinetic energy E'_{kin} can be calculated as follows

$$E'_{kin} = h\nu - E_{Bin} - \Phi_A \tag{3}$$

Unfortunately, the work function of the analyser is not known. Since a metal surface is measured the Fermi energy can be used to calibrate the measured kinetic energy. Using the formula 3, the Fermi energy can be calculated as follows:

$$E'_F = h\nu - 0 - \Phi_A \tag{4}$$
$$= h\nu - \Phi_A \tag{5}$$

Using the formulas 3 and 5 the binding energy of the measured electron can be calculated as follows:

$$E'_F - E'_{kin} = h\nu - \Phi_A - (h\nu - E_{Bin} - \Phi_A) \tag{6}$$
$$= E_{Bin} \tag{7}$$

This shows that the binding energy for surface spectra is independent of the photon energy as well as the work function of the surface and the analyser. To change the photon energy in the experiment, the monochromator is moved. Even if the monochromator is brought back to the previously measured energy, it cannot be assured that the same photon energy will be reached again. Since the Fermi energy depends on the photon energy, as shown by formula 5, the energy calibration must be repeated each time the monochromator is moved. To determine the Fermi energy in the experiment, the Fermi edge is recorded and fitted with a Gaussian error function, see Figure 6.

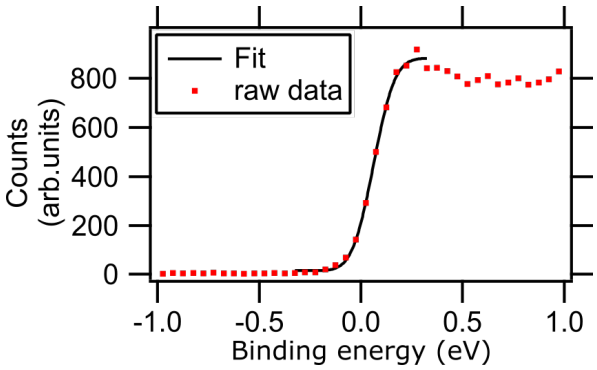

Figure 6: **Fitted Fermi edge for a photon energy of 750 eV**

For the gas phase measurements, the sample is retracted, so that now the gas molecules are measured. In contrast to the surface measurements, the electrons that are ejected from the gas phase do not have a Fermi energy. For the gas phase, the binding energy and the vacuum levels $E_{vacuum}(z)$, which are dependent on the molecule's location, determine the energy of the ejected electron [43]. This means that

$$E_{kin} = h\nu - (E_{Bin} - E_{vacuum}(z)) \tag{8}$$

Analog to the surface measurements, the analyser's work function impacts the measured kinetic energy E''_{kin}. [43]

$$E''_{kin} = h\nu - (E_{Bin} - E_{vacuum}(z)) - \phi_A \tag{9}$$

The vacuum level E_{vacuum} of the gas phase aligns with the surrounding material's work function. For the APXPS measurements, the probed area is very close to the surface, so it can be assumed that the vacuum levels are aligned with the work function of the surface. [43] So the equation gets simplified to:

$$E''_{kin} = h\nu - E_{Bin} - (\phi_A - \phi_S) \tag{10}$$

The ions that are created by photoemission also generate a field that affects the vacuum level, this effect is called space charging. This effect can be neglected since the experiment has a constant gas flow and also the value of the space charging can be regarded as constant. [43]

To calibrate the energy, the Fermi energy that was measured for the surface is used again:

$$E'_F - E''_{kin} = (h\nu - \Phi_A) - (h\nu - E_{Bin} - (\phi_A - \phi_S)) \tag{11}$$

$$= E_{Bin} - \Phi_S \tag{12}$$

This shows that the binding energy is dependent on the surface work function. This work function Φ_S changes depending on the surface coverage of the catalyst. This means that the gas phase electrons experience a different potential when the surface coverage changes, which influences the measured kinetic energy. Therefore, the kinetic energy of the gas phase peaks shifts by the same value as the surface potential changes.

4 Preparation

To prepare the Pt(111) crystal for the measurements it was sputtered for 20 min ($1{\cdot}10^{-5}$ mbar, 10 mA, 1 kV) and then annealed at 600 °C for 10 min. Equally, the palladium polycrystal was sputtered with Ar ($2.5{\cdot}10^{-5}$ mbar, 10 mA, 1 kV) for 25 min to clean the surface and then annealed at 700 °C (3.6 A, 200 V). This process was repeated three times for the polycrystal. After this, the crystal is moved from the preparation chamber to the analysis chamber. To prove that the sample is clean, surveys were recorded. The two recorded surveys for the Pd polycrystal show that the sample surface is clean except for a small amount of carbon.

4.1 Aligning of Pd polycrystal

The different grains of the polycrystal and their crystallographic orientation were determined in a previous study [30], see Figure 7 (a). This map is used to locate the different grains on the crystal by comparing it to a picture taken of the crystal in the sample holder, see Figure 7 (b). Through the different orientations of the grain, the grains have different reflectivities, which makes it possible to identify a few grains directly from the picture. Using grain P, which is especially easy to recognize, the map can now be rotationally aligned with the crystal.

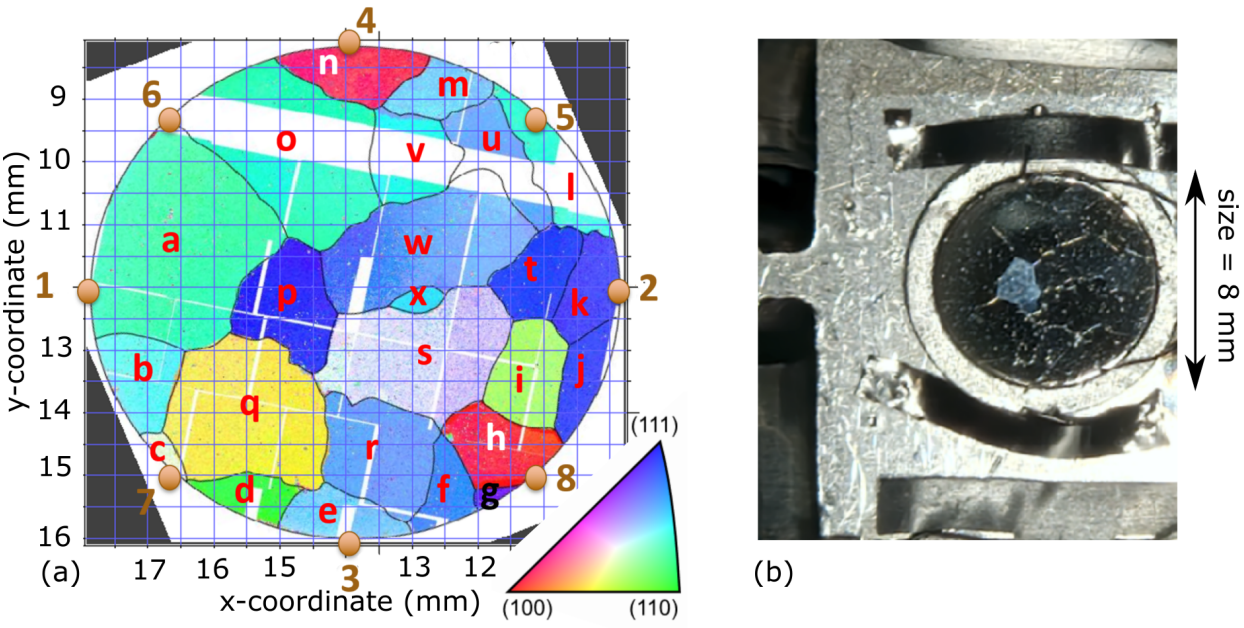

Figure 7: **Positions and alignment of the different grains on the polycrystal**, (a) Map of the different grains and crystallographic orientation coloured corresponding to the stereographic triangle. The figure is adapted from [30]. (b) Photography of the polycrystal

The next step is to determine the position of the edges of the polycrystal to be able to navigate the photon beam to the specific grains. For this, the analyser is brought into

position to measure the surface of the catalyst. Using the total number of electrons from the Pd $3d_{5/2}$ peak that reaches the analyser, makes it possible to determine whether the photon beam is hitting the sample. When the total number of detected electrons is reduced to half, the photon beam is roughly half on the crystal. This position is used to get the coordinates for the edges, marked with 1-4 in Figure 7 (a). To double-check our alignment of the crystal, the beam was also moved to positions 5, 6, 7, and 8 see Figure 7 (a). The position of the sample was also checked later in the measurements to ensure that the beam position was not influenced by the heating or by sample transfer out/into the AP Cell. The recorded spectra later proved that we can navigate on the crystal easily and are able to go back to previously measured positions easily with a precision of $\pm$ 50 μm.

4.2 Temperature oscillations

To oscillate the temperature an IR laser is used to heat the sample and a type K thermocouple is used to determine the temperature on the sample surface. When heating the sample the laser overshoots the setpoint temperature, but due to the fast temperature oscillation used for the experiments, the system does not have enough time to correct the overshoot of the temperature. This results in larger, but still periodic temperature oscillations, which does not affect the experiment.

5 Data analysis

The analysis method is illustrated using a previously measured CO oxidation dataset over Pt(111) while oscillating the temperature. For this, a gas composition of CO:O_2 of 2:4 sccm was used. To oscillate the catalyst between an active and inactive phase the temperature was varied between T = 283 °C and T = 381 °C with a period of 50 s, see Figure 9 (a).

The bottom of Figure 8 (a) shows the image plot of the energy-calibrated normalized time-resolved C 1s spectra of the gas phase measured over a Pt(111) surface while oscillating the temperature (i.e. the sample was retracted as shown in Figure 4 (b)). The top part of Figure 8 (a) will be explained later. Inspection of the bottom of the image plot of Figure 8 (a), shows two phases depending on the temperature. One phase where the catalyst is active, which only shows CO_2 in the gas phase and one when the catalyst is inactive, accompanied by a strong CO peak and a slightly shifted lower intensity CO_2 peak at 291.9 eV (marked with an arrow in Figure 8 (a)). In the remainder of this section, this peak will be referred to as the weak CO_2 peak. The changing gas composition influences the electron attenuation and consequently, the amount of measured electrons changes with the temperature. To correct the oscillating intensity caused by attenuation, the spectra need to be normalized. Since the experiment is done with a constant gas flow with a constant mixing ratio, the total number of C and O atoms in the gas phase remains the same, regardless of whether CO oxidation occurs or not. Therefore, I normalized the data to the sum of the CO and CO_2 signals in each spectrum. In practice, this is done by integrating the binding energies between 289.5 eV and 292.6 eV for each spectrum. Each spectrum is then divided by this value.

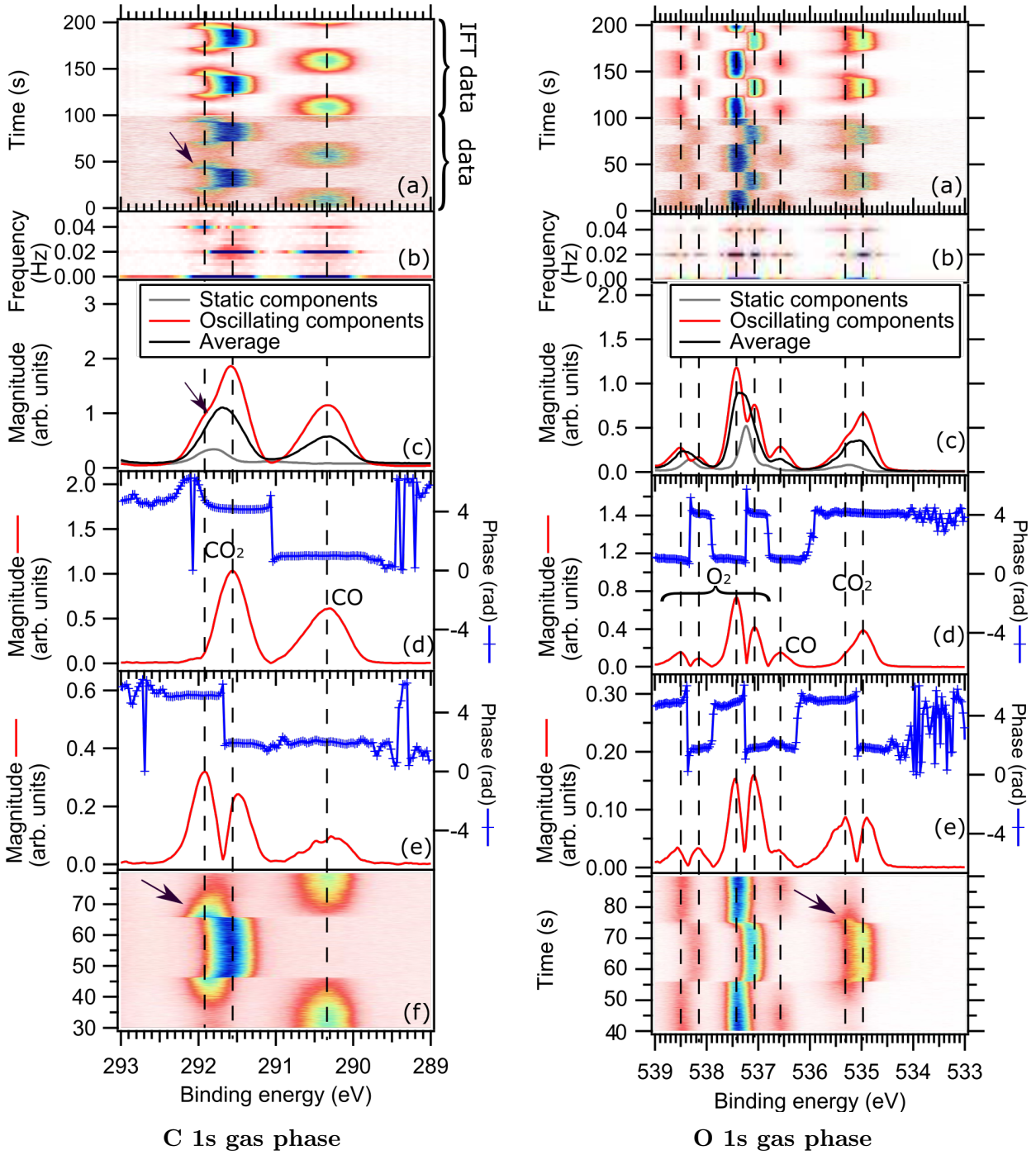

Figure 8: **Image plot and Fourier transform of time-resolved C 1s/O 1s gas phase spectra**, photon energy 750 eV, CO:O_2 of 2:4 sccm, temperature oscillation between T = 283°C and T = 381°C with a period of 50 s, (a)/(g) Image plot (top half: inverse Fourier transform without 0 Hz, bottom half: energy-corrected normalized data) (b)/(h) Oscillation amplitude as a function of frequency and E_{Bin} (c)/(i) Comparison of the oscillating component, the static components and the time average of the image plot (d)/(j) 0.02 Hz oscillation amplitude and phase spectrum (e)/(k) 0.04 Hz oscillation amplitude and phase spectrum (f)/(l) Event average data

5.1 Fourier transformation

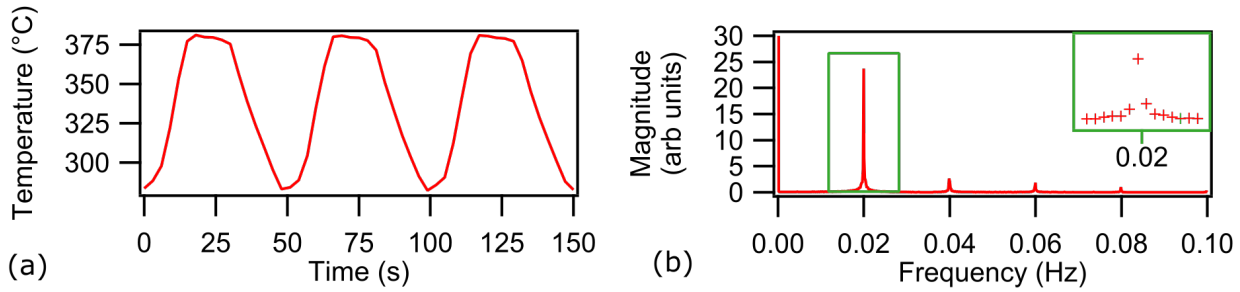

Figure 9: **Temperature oscillations** (a) Temperature data (b) FT

When integrating over the whole image plot, the resulting CO_2 peak is a superposition of the CO_2 and the weak CO_2 peak, see black spectra in Figure 8 (c). To get a better resolution of the oscillating components, each binding energy channel is Fourier transformed along the time axis. This results in a plot of the oscillation amplitude as a function of frequency for each binding energy channel, see Figure 8 (b). In this plot, a clear frequency component is observed at 0.02 Hz. This corresponds to the driving frequency of the temperature oscillation, $f = \frac{1}{T} = \frac{1}{50\ \mathrm{s}} = 0.02$ Hz, see Figure 9 (b). In addition to information about the oscillation amplitude at different frequencies and binding energies, the Fourier transformation also gives information about the phase of each oscillating component. Figure 8 (d) shows both the magnitude and the phase of the 0.02 Hz signal.

The upper panel of Figure 8 (a) shows the inverse Fourier transform (IFT) using 20 harmonics (0.02 Hz, 0.04 Hz, 0.06 Hz, and so on), excluding the 0 Hz component. Why I excluded the 0 Hz component will be explained later. A comparison between the

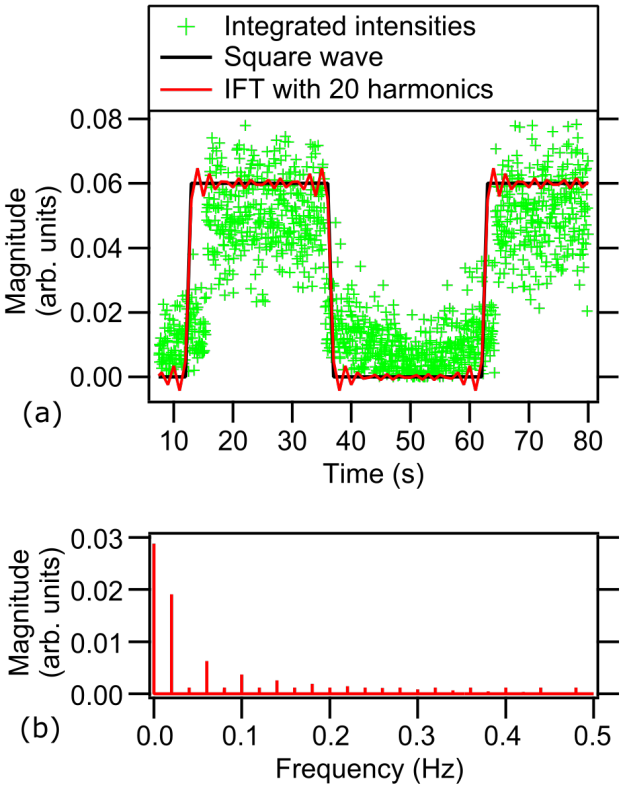

Figure 10: **Fourier and inverse Fourier transform for a square wave**, (a) Fourier transformation of a square wave (b) Green: Integrated intensities at $E_{Bin} = 291.6$ eV along the time axis of the C 1s gas phase spectra, black: Square wave, red: inverse Fourier transform regarding the 0 Hz component and the first 20 harmonics

original image plot and the inverse Fourier transform shows that the two plots look very similar, but the inverse Fourier transform is a bit blurred. This can be explained by taking a closer look at the image plot for the C 1s spectra in Figure 8 (a) and at the event averaged data in (f), which will be explained later. For example, it can be seen that the CO_2 peak changes between a high and nearly zero intensity very abruptly when the temperature changes. The green markers in Figure 10 (a) show the intensities progression of the CO_2 peak at 291.6 eV as a function of time. Looking at the curve it can be seen that it resembles a square wave (black). When doing the Fourier transform of a square wave, see Figure 10 (b), an infinite amount of sine functions are needed to describe the wave. Figure 10 (a) shows the inverse Fourier transformation of a square wave using 20 harmonics of the FT and the 0 Hz component. Clearly, it reproduces the square wave relatively well, but the corners are not matched perfectly. This causes the inverse Fourier transformation to appear slightly blurred when compared to the original image plot, as seen in Figure 8 (a).

Another important factor to consider is the sampling frequency. To illustrate this the following sine function is considered: $f(x) = 0.5 \cdot sin(2\pi \cdot 0.02\ \text{Hz} \cdot x + \frac{\pi}{4}) + 1$ with a frequency of 0.02 Hz, an oscillation amplitude of 0.5, a phase shift of $\frac{\pi}{4}$ and a vertical shift of 1, sampled with 0.1 s or 0.07654 s, respectively. The sampling does not affect the appearance of the sine wave in real space much, but upon Fourier transformation, differences become clear in frequency space. This is evident by comparing the Fourier transform of the sine waves. While the FT sine wave sampled with 0.1 s shows the expected oscillation amplitude, the FT of the other shows a slightly shifted and wider peak with a lower intensity, see Figure 11 (a). In the following I will refer to the data points next to the main as sidebands.

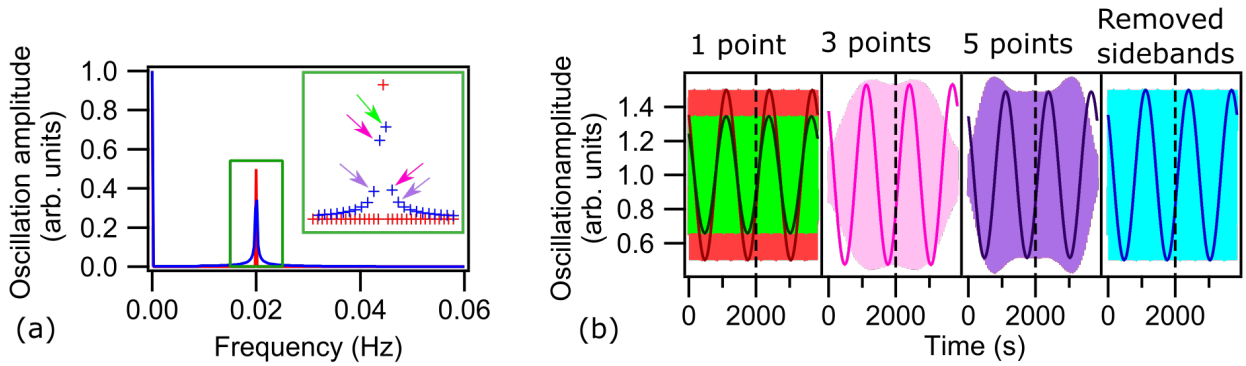

Figure 11: **Fourier transform of a sine wave and amplitude modulation in inverse Fourier transform considering different amounts of points from the sidebands** (a) Fourier transform with 0.1 s sampling period (red) and 0.07654 s sampling period (blue) (b) "Shape" of amplitude modulation superimposed with extracted curve from black dashed line for red: sampling difference of 0.1 s, green: sampling difference of 0.07654 s only considering peak point (marked with green arrow in (a)), pink: sampling difference of 0.07654 s considering peak point and first point from sidebands on each side (marked with green and pink arrows in (a)), purple: sampling difference of 0.07654 s considering peak point and first two points from sidebands on each side (marked with green, pink and purple arrows in (a)), blue: sampling difference of 0.07654 s with removed sidebands

Also, in the inverse Fourier transformation, the different sampling frequencies lead to observed differences. While the red data points sampled with 0.1 s perfectly reproduced the oscillation amplitude with only one Fourier-transformed data point, the data sampled with 0.07654 s, was shown to be strongly dependent on the number of considered points from the sidebands. The comparison in Figure 11 (b) of IFT using 1, 3, and 5 points of the FT data around the 0.02 Hz signal shows that the curve is better and better reproduced if more sidebands are included.

The reason for the sidebands is that the Fourier transform assumes that the initial and final measurements probe the same point of the oscillation period. This assumption is not fulfilled in practice and most often the first and last measured points are not matching. This disruption of the periodicity leads to the observed sidebands. Since the sidebands have a significant influence on the data reconstruction – as shown here - it is important to consider this and either include enough sidebands for the inverse FT or ensure that the initial and final measurements probe the same point in the raw data which effectively remove all sidebands in the FT-data. The advantage of the removal of the sidebands is that the original wave is reconstructed without needing to consider edge effects caused by amplitude modulations, see the blue curve in Figure 11 (b). [29] Therefore I decided, analog to the data analysis in Ref. [29], to remove the sidebands. To do this the Fourier transformed temperature data, see Figure 9, is used to determine the exact oscillation period. This makes it possible to determine how many full periods were measured in each dataset to then cut the "additional" spectra off.

To synchronize the measurements of different core levels the starting time of each measurement is adjusted in such a way that each experiment starts exactly at the same time point in the temperature oscillation. This proved to be slightly complicated since the removal of the sidebands requires that the length be equal to a finite number of complete temperature oscillations. Therefore, one cannot remove the first spectra of the measurement to achieve the same starting time for the different spectra, since this would change the length of the image plot and thus create sidebands. Instead one can take advantage of the periodicity of the experiment. After the removal of the sidebands, the initial and final spectra of the measurement measure the exact same point of the oscillation period. Therefore, the spectra that need to be removed at the beginning of the measurement to reach the same starting point for all experiments, can simply be added to the end of the image plot, without creating sidebands.

To now compare the different time-aligned image plots with each other the inverse Fourier transform without the 0 Hz component is used. This has the benefit that the produced image plot only shows the oscillating components since the 0 Hz component that gives information about the average signal is not included. This results in a plot of the changing components that now are oscillating around zero since the average was removed. To get a better picture of the oscillation spectrum, the minimum value for each binding energy was determined and then added to all values of the individual binding energy. This has the advantage that the resulting image plot still only shows the oscillating peaks, but which now oscillate between the maximum reached intensity and zero for each binding energy. A further advantage of

using the inverse FT without the 0 Hz component is that the time evolution of the observed peak can be observed directly. In the following, I will call the inverse Fourier transform image plot without the 0 Hz component, IFT image plot.

Another interesting observation is how much of the gas phase or surface is oscillating. To illustrate this the inverse Fourier transformation was done including the 0 Hz component. Now for each binding energy the minimum and the maximum value was identified. This makes it possible to determine the total oscillation strength for each binding energy by subtracting the lowest measured intensity (i.e. the static component) from the highest measured intensity for each binding energy. Figure 8 (c) shows the static component in grey, the oscillating component in red, and the time average, which is gained from integrating over the whole image plot in black.

5.2 Event averaging

Another technique used to analyse time-resolved data is event averaging. This technique addresses the low signal-to-noise ratio caused by the very short measurement time of each spectrum needed to get good time resolution. To solve this problem the event is repeated multiple times. To be able to event average the data, two internal signals are needed to identify at which point the two phases are starting/ending. In this case, when looking at the image plot in Figure 8 (a) it can be seen that at the beginning and end of the active phase, there is a binding energy change in the CO_2 peak. This shift is used to identify at what exact moment the catalytic active phase starts and ends. Since these two events happen at every repetition of the experiment, they can be used as triggers to average the data over multiple repetitions. The event averaged data in Figure 8 (f) and (l) clearly show that this technique makes it possible to reach a high time resolution with a good signal-to-noise ratio. More details about the procedure can be found in reference [24].

5.3 Application of Fourier transform on Pt(111) data

Coming back to the data analysis of the C 1s gas phase spectra in Figure 8, the Fourier transform of the image plot in panels (b) clearly shows two strong components at 0.02 Hz, i.e. the gas phase is oscillating with the driving frequency of the temperature oscillation. When extracting the 0.02 Hz spectra, see Figure 8 (d) it can be seen that the CO and the largest CO_2 peak appear alternating since they have a phase shift of π, consistent with the observation from the real space in the image plot and the IFT image plot in Figure 8 (a). This behaviour is caused by the temperature oscillations that cause the catalyst surface to be less and more active.

When only looking at the 0.02 Hz spectrum it can be seen that the weak CO_2 peak cannot be found. This can be explained by looking back at the image plot. There it is clearly seen that the weak CO_2 peak (marked with a black arrow) in Figure 8 (a) always appears before and after the large CO_2 peak and therefore appears twice as often, meaning it appears with

double the frequency as the other peaks. This is mirrored in the 0.04 Hz spectrum of the Fourier transform (Figure 8 (e)) which clearly shows the weak CO_2 component.

The appearance of the weaker work function shifted CO_2 peak before and after the maximum of the CO peak, could be a sign of a potential highly active third phase existing since the CO_2 production starts before the change of the catalyst surface. To verify the existence of another phase, the surface spectra, which will be discussed later, are needed.

The same observation of the CO (at 536.5 eV) and the two CO_2(at 535 eV and 535.3 eV) peaks can also be made in the O 1s oscillation amplitude spectra in the gas phase, see Figure 8 (j) and (k). The O 1s gas phase 0.02 Hz oscillation amplitude spectrum additionally shows the peaks of the O_2 doublet, at 538.5 eV and 537.4 eV, as well as the work function, shifted O_2 peaks at 538.2 eV and 537.1 eV, respectively. The phase value shows that the peaks of the O_2 doublet are in phase with CO, and appear alternating with the work function shifted O_2 which are in phase with the largest CO_2 peak. The absence of a work function-shifted CO peak in phase with the largest CO_2 indicates complete combustion of CO. This can also be seen when looking at the static component (grey) in Figure 8 (c) and (i), which clearly shows that the static component is zero for the CO peak, while a strong oscillating component (red) can be observed. That proves that the surface oscillates between a structure that converts no and 100% of all CO reaching the surface. In other words, the surface oscillates into and out of the CO mass transfer limit (CO-MTL).

Contrary to the gas phase spectra the O 1s and C 1s surface spectra cannot be normalized to the total amount of O/C atoms, since the number of adsorbed O and C on the surface is not constant. Therefore, the C 1s and O 1s surface spectra are normalized to the secondary electron background.

When looking at the image plot of the C 1s surface spectra in the lower half of panel (a) in Figure 12 the oscillating components are nearly impossible to see due to the relatively low intensity in comparison to the background noise. This can also be seen in Figure 12 (c) when comparing the static components (grey) with the oscillating components (red). However, the 0.02 Hz oscillation amplitude spectrum in Figure 12 (d) as well as the IFT image plot in the top part of (a) clearly shows two oscillating peaks. These two peaks are caused by the different bonding positions of the CO on the surface, CO adsorbed in the top position at 286.5 eV and CO adsorbed to the bridge site at 285.9 eV [44]. The phase values of the two peaks show that they occur simultaneously. A careful inspection of the phase values of the C 1s surface spectra, see Figure 12 (d), shows one additional peak at around 291.4 eV (marked with a red arrow), with a phase shift of π compared with the two surface peaks. This peak can be identified as the CO_2 peak that was also observed in the gas phase spectra in Figure 8 (d).

The two peaks assigned to these two different adsorption sites can also be identified in the O 1s oscillation amplitude spectrum. Here the peak at 532.4 and 531 eV are assigned to top and bridge bonded CO, while the additional peak at 529.5 eV is assigned to adsorbed oxygen in the hollow site [44]. The left side of the spectrum shows the gas phase peaks, that were already determined before. The phase values show that the CO_2 peak appears

simultaneously with adsorbed O, while in anti-phase the two adsorbed CO peaks, see Figure 12 (i). This proves that part of the catalyst's surface is alternating between oxygen-covered, while the catalyst is in the MTL, and CO-covered when the catalyst is inactive.

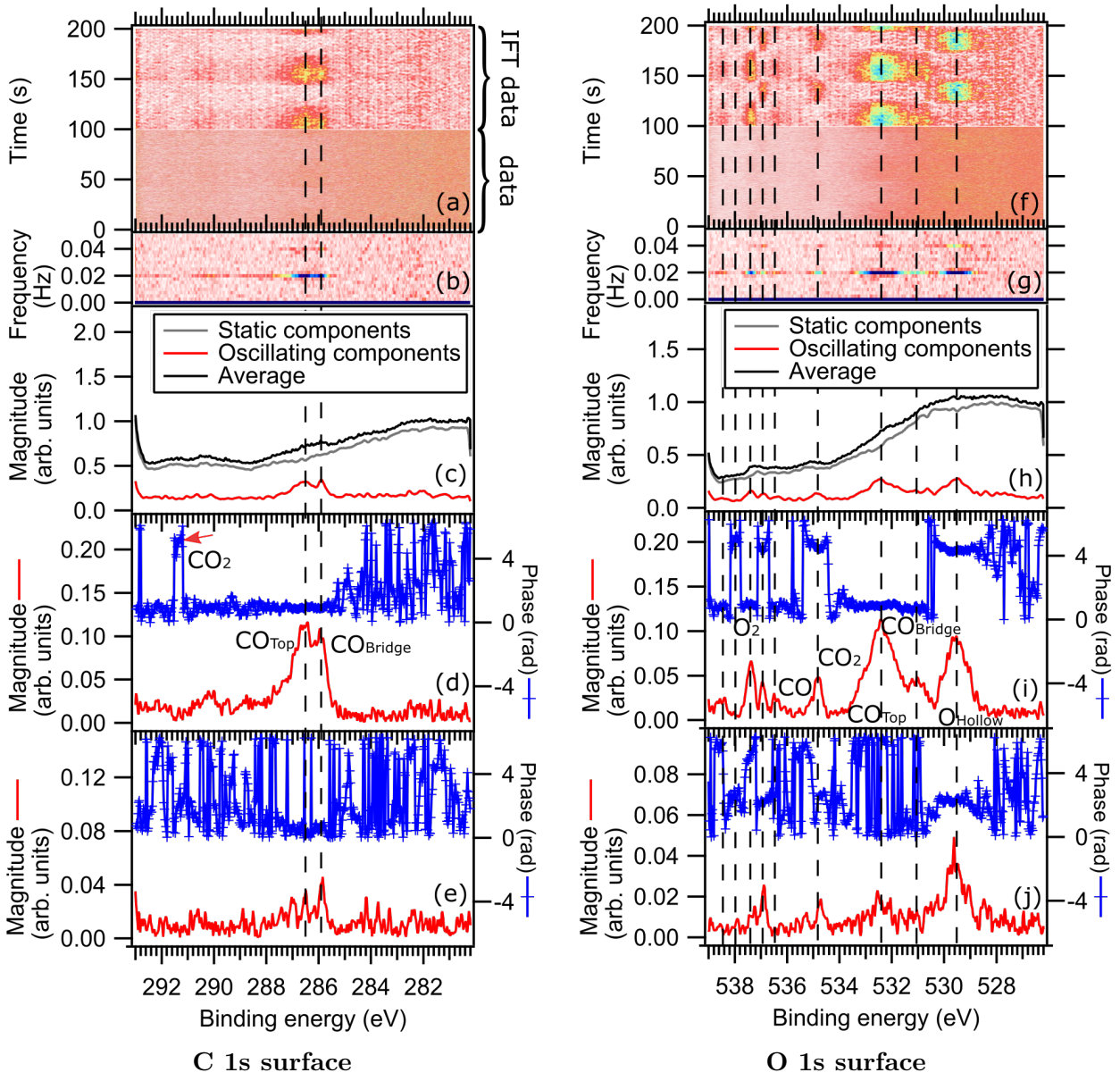

Figure 12: **Image plot and Fourier transform of time-resolved C 1s/O 1s surface spectra**, photon energy 750 eV, CO:O_2 of 2:4 sccm, temperature oscillation between T = 283°C and T = 381°C with a period of 50 s, (a)/(f) Image plot (top half: inverse Fourier transform without 0 Hz, bottom half: energy-corrected normalized data) (b)/(g) Oscillation amplitude as a function of frequency and E_{Bin} (c)/(h) Comparison of the oscillating component, the static components and the time average of the image plot (d)/(i) 0.02 Hz oscillation amplitude and phase spectrum (e)/(j) 0.04 Hz oscillation amplitude and phase spectrum

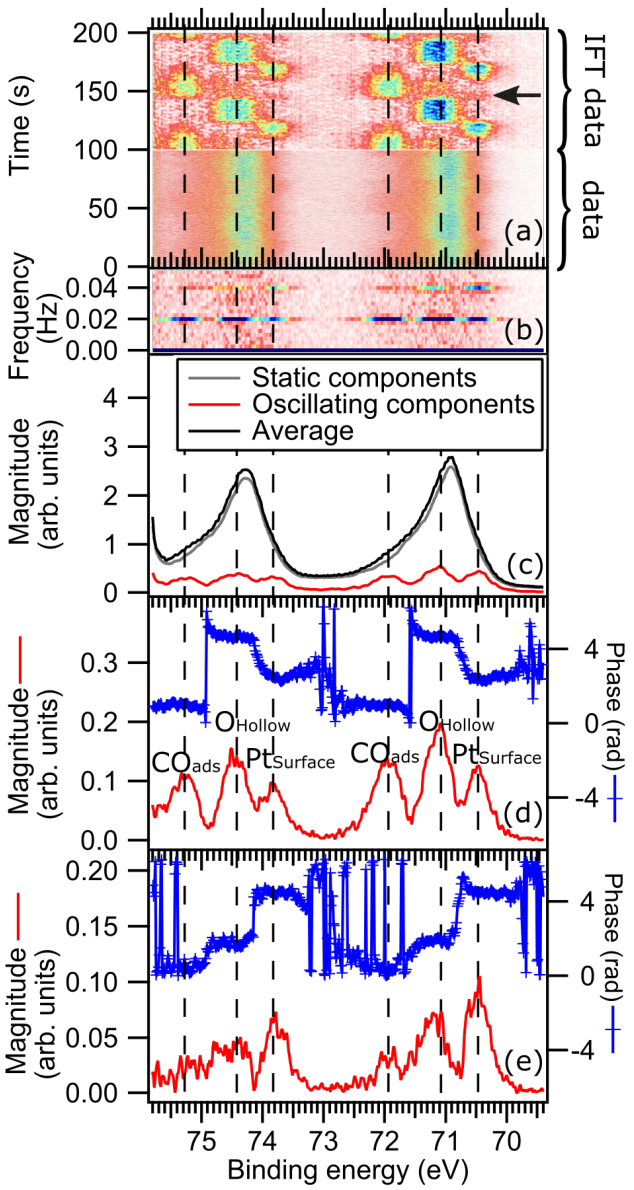

Figure 13: **Image plot and FT of time-resolved Pt 4f surface spectra**, $h\nu$=390 eV, CO:O_2 of 2:4 sccm, temperature oscillations: T = 283°C (25 s) and T = 381°C with a period of 50 s, (a) Image plot (top half: IFT without 0 Hz component, bottom half: energy-corrected normalized data) (b) Oscillation amplitude as a function of frequency and E_{Bin} (c) Comparison of the oscillating components, the static components and the time average of the image plot (e)/(f) 0.02 Hz/0.04 Hz oscillation amplitude and phase spectrum

When comparing the 0.02 Hz oscillation amplitude spectra for the C 1s and O 1s surface spectra, in Figure 12 (d) and (i), a different intensity distribution between the peaks for the CO adsorbed on top and at the bridge site can be seen. A possible explanation could be that as seen in Figure 12 (d) the two peaks in C 1s spectra overlap strongly, consequently influencing the measured maximum intensity of the single peaks. In contrast to that the same two peaks in the O 1s spectra have a larger separation and, as a result, do not overlap so much, see Figure 12 (i).

The last spectra to discuss are the Pt 4f surface spectra. These spectra were normalized to the total amount of Pt atoms assuming that the amount of probed Pt atoms stays constant independently of the changing surface coverage of the catalyst. The image plot of the Pt 4f surface spectra, in the bottom panel of Figure 13 (a) and the average over the image plot shown in Figure 13 (c) (black graph) shows two prominent peaks with intensities of 70.9 eV and 74.3 eV. Comparing these binding energies to paper [44], they agree with the bulk components of Pt from the $4f_{5/2}$ and $4f_{7/2}$. These components cannot be found in the IFT image plot proving that the bulk is not oscillating as expected.

The oscillating peaks in Figure 13 (d) can be assigned to clean Pt(111) at 70.5 eV ($Pt_{surface}$) and CO on top of Pt(111) either (4×4) or c(4×2) with a binding energy of 71.9 eV (CO_{Top}). The middle peak at 71.1 eV could be either O adsorbed to the hollow site (expected at 71.1 eV) or CO adsorbed to

the bridge site (expected at 71.2 eV) [44]. Since the predicted binding energy of both peaks is very close, it is expected to only observe the most intense component. The phase values show that the observed peak is in antiphase with CO adsorbed to the bridge site. Together with the information from the O 1s surface spectra, that shows that CO_{Top} and CO_{Bridge} are in phase and appear alternating with O_{Hollow}, it can be concluded that the observed peak at 71.1 eV is primarily oxygen adsorbed in the hollow site. Interestingly, the phase values also reveal that the $Pt_{surface}$ peak has a phase value in between the CO_{ads} and the O_{Hollow}. This implies that there are three stages/phases. These three stages can also be seen very clearly in the inverse Fourier transform without the 0 Hz component of the image plot in the top panel of Figure 13 (a). The IFT image plot clearly shows that $Pt_{Surface}$ peak appears with a relatively large intensity when the surface is changing from CO to O-covered. A closer look at the IFT image plot also shows that there is also a $Pt_{Surface}$ component with a much lower intensity when the surface is changing from O covered to CO covered, see Figure 13 (a).

When comparing these results to the event-averaged data of the gas phase spectra in Figure 8 (f) and (l), it can be seen that the appearance of the clean Pt surface matches the earlier observed work function shifted CO_2 peak, which also appears with double the driving frequency. Contrary to the observed intensity of the Pt peaks, the work function shifted CO_2 peak does not show a large intensity difference. This could be because the low-intensity Pt surface peak occurs when the surface changes from O to CO. This means the catalyst changes from active to CO poisoning. Consequently, there could still be some CO_2 left in the gas phase from when the catalyst was active, which has not been pumped away yet. This leftover CO_2 would also be affected by the work function shift and so be the reason for the strong work function shifted CO_2 even though only a small amount of clean Pt surface is appearing.

The CO and O-covered phases depending on the temperature were also found in a previous paper [45]. In this previous study, a mixing ratio of 9:1 of O_2: CO was used, with a total pressure of 0.25 mbar with a constant flow rate of 1.35 – 1.4 sccm. This previous study also utilized APXPS to study the surface coverage of Pt(111) in dependence on temperature. By stepwise increasing the temperature by 25 - 50 K, it was discovered that the surface of the catalyst transforms rapidly from CO-poisoned to O-covered at 535 K. The study concluded that the shift between the two phases is sudden and there is no phase where adsorbed O and CO coexist on the surface.

The CO and O-covered phases were also confirmed by my measurements. The use of time-resolved measurements and the Fourier transform made it, however, possible to observe that for a short amount of time, a third highly active clean Pt surface exits. This transition phase appears at a high intensity when the surface is changing from CO to O covered and at a lower intensity when the surface is changing from O to CO covered.

6 Palladium Polycrystal

For the first two experiments on the Pd polycrystal, a 2:2 sccm gas composition of CO:O_2 and a total pressure of 2.03 mbar were used. For the first experiment, the influence of the size

of the temperature oscillations on the surface coverage was studied on the same grain. For the second experiment, the temperature was varied between 233 °C and 293 °C with a period of 30 s to stay within the CO-MTL and different CO-covered grains were compared. For the third experiment, the temperature oscillation was increased to 170 °C and 278 °C with a period of 55 s with a gas composition of 1:3 sccm $CO:O_2$ to go into and out of the CO-MTL.

For the data analysis of the palladium polycrystal, the same steps were followed as explained for the Pt(111) crystal, with two additional steps.

The first additional step is to correct the image plot for the transmission function of the electron analyser. This is an essential step due to detector imperfections and variations in electron transmission through the electron analyser, depending on the E_{kin} of the electron and the chosen pass energy. The detector has two modes of operation: swept mode and snapshot mode. To enable time-resolved measurements the snapshot mode of the electron analyser is used. In this mode, the analyser has a set pass energy and constant retarding voltage for the kinetic energy of the incoming photoelectron. With each measurement, the intensity distribution on the screen is measured. This means that for each measurement the same pixel always measures the intensity for the same kinetic energy. To correct for the slight intensity variation due to detector imperfection as well as for the analyser itself a swept image is measured. When in swept mode, the detector automatically adjusts the retarding voltage so that each pixel measures every kinetic energy. The swept spectra thus provide the real intensity distribution. To now correct the intensity distribution of the snapshot mode, a transmission function is defined. To get the transmission function the value of the integrated swept mode image is divided by the value of the integrated snapshot image for each binding energy. To transmission correct the image plot, each snapshot mode spectra are now multiplied with this transmission function. This data processing step was not done previously for the Pt(111), since unfortunately no swept spectra were measured.

The second additional step consists of removing the secondary electron background. This is necessary since, when normalizing the energy and transmission corrected image plot to the total amount of Pd atoms, it is apparent that the secondary electron background oscillates strongly with the temperature, see right side of Figure 14 (a). This is due to the change in the gas composition depending on the temperature. Since the different gas compositions have different electron attenuation, the amount of measured electrons oscillates as well. To remove the oscillating background created by the secondary electrons, the background must be fitted for each individual spectrum. To fit the background an 8^{th} order polynomial is used, see Figure 14 (c). As the first step the integrated image plot is fitted with the help of a weight function to get values for the initial guess of the fitting parameter for the first spectrum. For the following spectra, the fitting values from the previous spectra are used as initial guesses. After fitting all spectra the background is subtracted individually for each spectrum. Now the spectrum can be normalized to the total amount of Pd atoms, as in the previous experiment with Pt(111). Looking at Figure 14 (b) it is evident that the background was successfully removed, since now only the peaks show an oscillating behaviour.

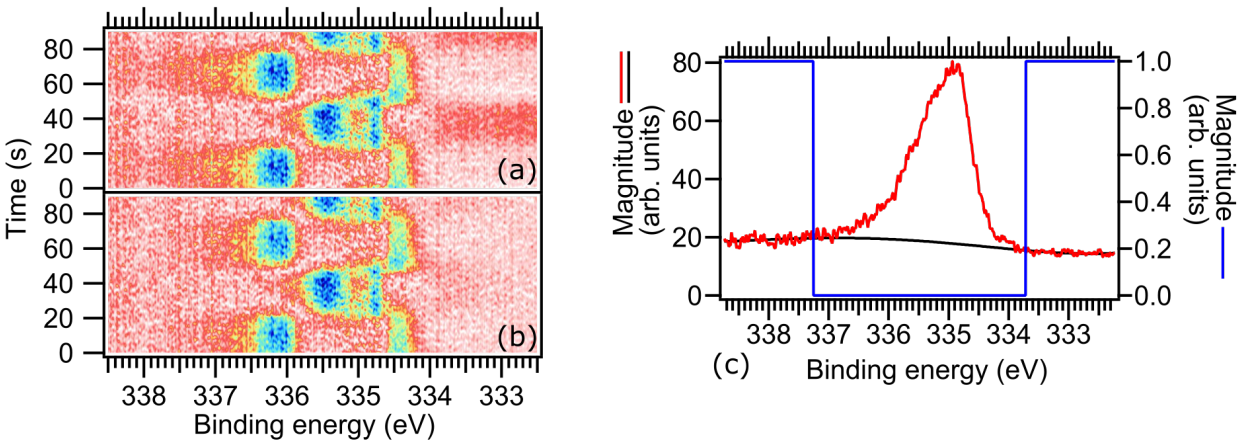

Figure 14: **Comparison IFT image plot with and without background removal** 3:1 O_2:CO, Temperature oscillation between T = 170°C and T = 278°C with a period of 55 s, Pd(100) (N grain) (a) without background removal (b) with background removal (c) Fitted background for the average of a Pd $3d_{5/2}$ image plot, red: average of Image plot, blue: weight function, black: background fit

The normalization of the spectra was done identically to the measurements on the Pt(111) crystal, meaning Pd spectra are normalized to the total amount of Pd atoms. Since this experiment also has a constant gas flow and pressure, it can be assumed that the total amount of C and O atoms in the gas phase is constant as well. This means that the C 1s and O 1s gas phase spectra can be normalized to the total amount of C or O atoms as well.

The number of adsorbed C and O atoms on the surface is of course not constant. Because of this the C 1s and O 1s surface spectra are normalized to the secondary electron background.

6.1 Temperature oscillations on CO-poisoned Pd(110)

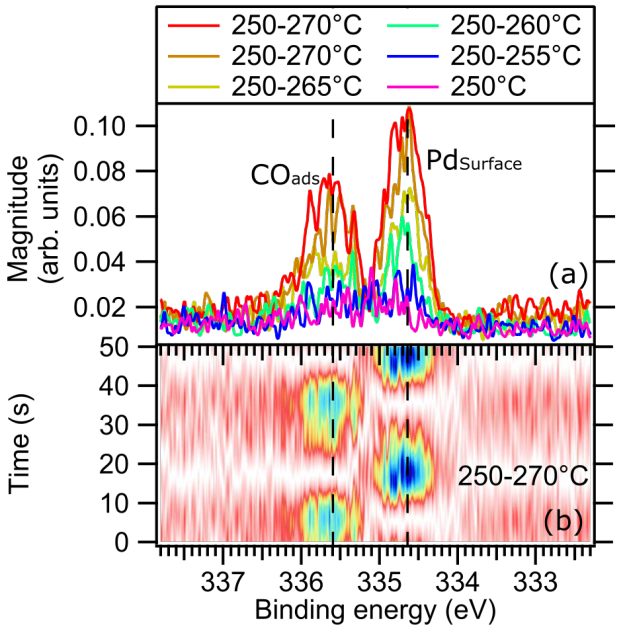

Figure 15: **Pd $3d_{5/2}$ surface**, Different Temperature oscillations on grain A (Pd(110)) (a) Comparison of Oscillation amplitude spectra for different temperature oscillations (b) IFT image plot (4 harmonics), Temperature oscillations between T = 250 °C and T = 270 °C with a period of 30 s

The first experiment studied the influence of different temperature oscillations on the same grain with a gas composition of 2:2 CO: O_2 at 2.03 mbar while staying in the CO-poisoned state. For this, the A grain was chosen, which has a structure close to a Pd(110) surface. Initially, the surface was measured at a constant temperature of 250°C. The oscillation amplitude spectrum clearly shows that only noise can be seen at a constant temperature, see the pink graph in Figure 15 (a). The temperature oscillations were then started between 250°C and 255°C (with a period of 30 s) and gradually increased by 5°C after each measurement until they reached 250-270°C. The two peaks that can be seen in Figure 15 (a), can be identified as CO adsorbed to Pd surface (CO_{ads}) at 335.6 eV and to a clean Pd surface ($Pd_{Surface}$) at 334.6 eV, in comparison with the paper [46]. For the IFT image plot in Figure 15 (b) I chose to only consider 4 harmonics of the FT for the inverse Fourier transformation since the spectra are very noisy and considering more harmonics would only add more noise. The IFT imageplot also clearly shows that CO_{ads} and $Pd_{Surface}$ appear alternating, see Figure 15 (b). As expected, larger temperature oscillations cause more of the surface coverage to oscillate. This means more vacancies are opening up on the surface the higher the temperatures are getting. The oscillation amplitude spectra in Figure 15 (a) clearly show that for all studied temperature oscillation only two peaks of $Pd_{Surface}$ and CO_{ads} can be observed, showing that no oxygen is getting adsorbed to the surface. This implies that the used temperature oscillations are not high enough for oxygen to adsorb to the surface.

6.2 Comparison of different grains in CO poisoned state

To compare the catalytic activity for different crystallographic orientations, different grains were compared for the same temperature oscillations. The temperature used in this experiment was selected to keep the grains in the CO-poisoned state for the duration of the measurements. To accomplish this, temperature oscillations between 233 °C and 293 °C with a period of 30 s at a pressure of 2.03 mbar and a gas composition of 2:2 sccm CO:O_2 were chosen. This results in a driving frequency of $f = \frac{1}{30\text{ s}} \approx 0.033$ Hz in the experiment, see

Figure 16. Measurements were taken for grains A, N, P, Q, D, S, and H (in this order). The Pd $3d_{5/2}$ spectra as well as the C 1s and O 1s spectra for the surface and the gas phase were measured. The O 1s surface spectra were unfortunately too noisy to obtain conclusive results and therefore will not be included in the following analysis.

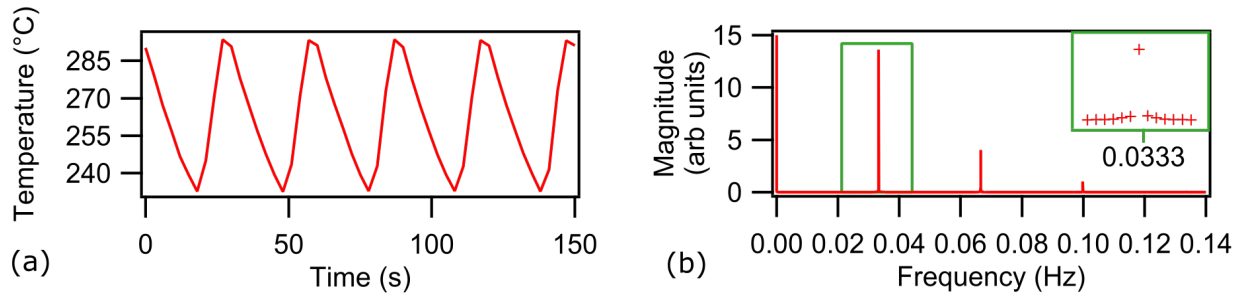

Figure 16: **Temperature oscillations** (a) Temperature data (b) FT

First, the N grain will be discussed in detail, which has a crystallographic orientation of (100). The papers [24, 33, 47] are used to identify the different peaks. The measured C 1s and O 1s gas phase spectra are displayed in Figure 17. The bottom part of (a) and (e) shows the energy, and transmission-corrected raw data, while the upper panel shows the inverse Fourier transformed data without the 0 Hz component (IFT image plot). Panel (b) and (f) show the oscillation amplitude as a function of frequency and E_{Bin}. Panels (c) and (g) show the oscillating (red), and static (grey) components of the measurement, as well as the time average (black) of the image plot. The fitted peaks of the 0.033 Hz component are displayed together with the corresponding phase values in Figures (d) and (h).

It is evident from comparing the magnitudes in Figure 17 (c) and (g) that the oscillations (red) are small in comparison to the static components (grey), while the spectra show large static CO and O_2 components (grey) only a much smaller oscillating CO_2 components (red) can be observed. This indicates that just a portion of CO in the gas phase is converted into CO_2, confirming that the measurements were taken in the CO-poisoned state of the catalyst. The oscillation amplitude of the CO_2 peak is the only one that nearly has the same intensity as the time average of the image plot, as seen in Figure 17 (c) and (g). This is also evident in the raw data in (a), which clearly shows that the CO_2 peak oscillates between very low and maximum intensity. This indicates that the catalyst surface is oscillating between a CO-poisoned surface with very low catalytic activity and a more active, yet still CO-poisoned surface.

The spectra in Figure 17 (d) show two components: a CO peak at 290.1 eV and a CO_2 peak at 291.7 eV. A closer look at the CO peak also shows the vibrational components of the CO molecule on the left side of the peak, marked with grey arrows in Figure 17 (d). The CO and CO_2 peaks have a phase shift of approximately π, meaning they appear alternating as expected. This can also be observed in the O 1s spectra in (h). Additionally to the CO_2 peak at 535.3 eV and the CO peak at 536.5 eV, the O 1s spectra also show the O_2 doublet at 537.2 eV and 538.3 eV. The phase value of the peaks proves that the two oxygen peaks

are as expected in phase with the CO peak. A closer look at the phase values shows that left to the stronger peak of the oxygen doublet at 537.2 eV is a small change in the phase value, marked with green arrows in Figure 17 (h). This phase shift of approximately 0.4 eV located at 537.6 eV is due to the work function shift when the surface coverage is changing. The shifted oxygen peak can only be seen in the phase values and not in the oscillation amplitudes, this implies that the work function shifted peaks have a very low intensity.

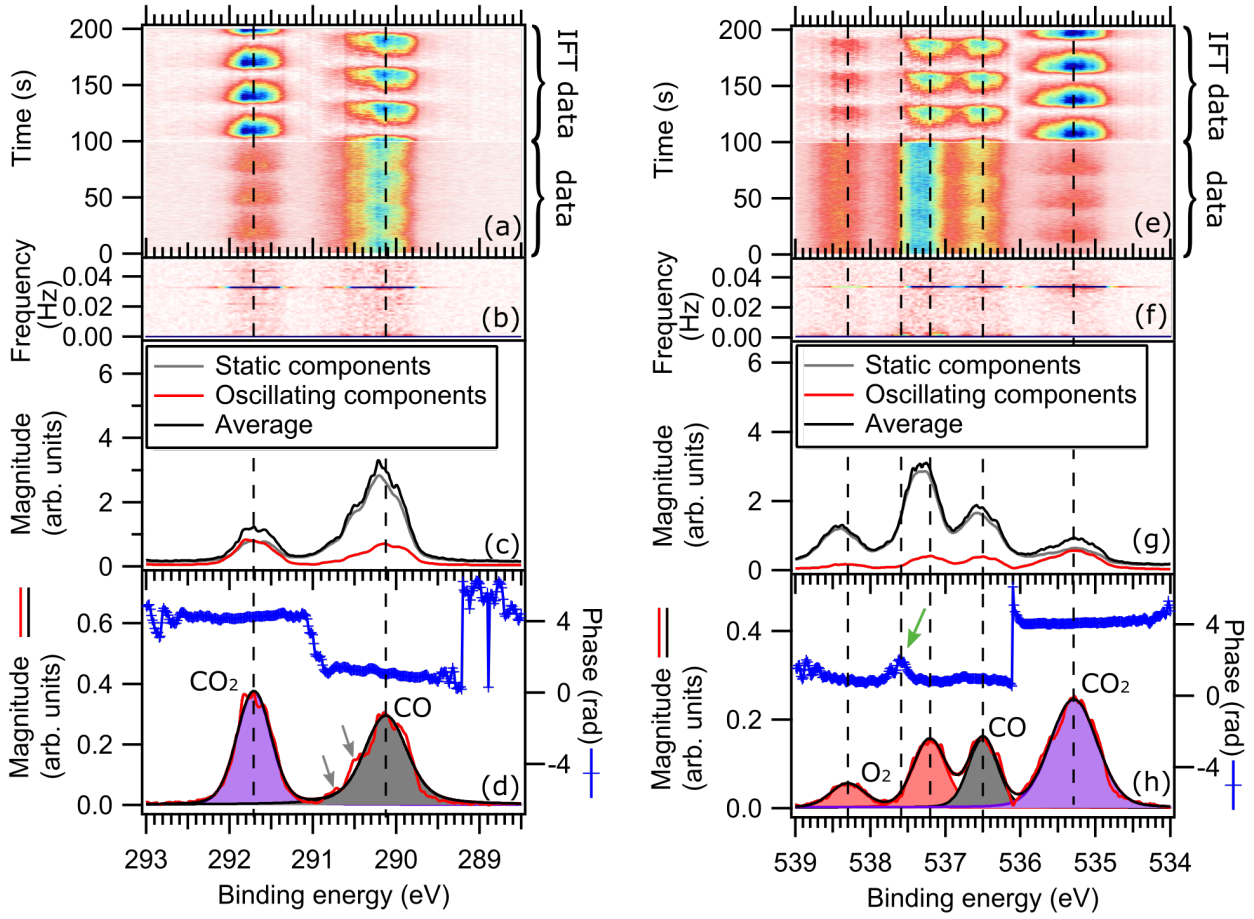

Figure 17: **Image plot and Fourier transform of time-resolved C 1s/O 1s gas phase spectra**, photon energy 510 eV/650 eV, CO:O_2 of 2:2 sccm, temperature oscillation between T = 233°C and T = 293°C with a period of 30 s, (a)/(e) Image plot (top half: IFT image plot (20 harmonics), bottom half: transmission-corrected normalized data) (b)/(f) Oscillation amplitude as a function of frequency and E_{Bin} (c)/(g) Comparison of the oscillating component, the static components and the time average of the image plot (d)/(h) 0.033 Hz oscillation amplitude and phase spectrum

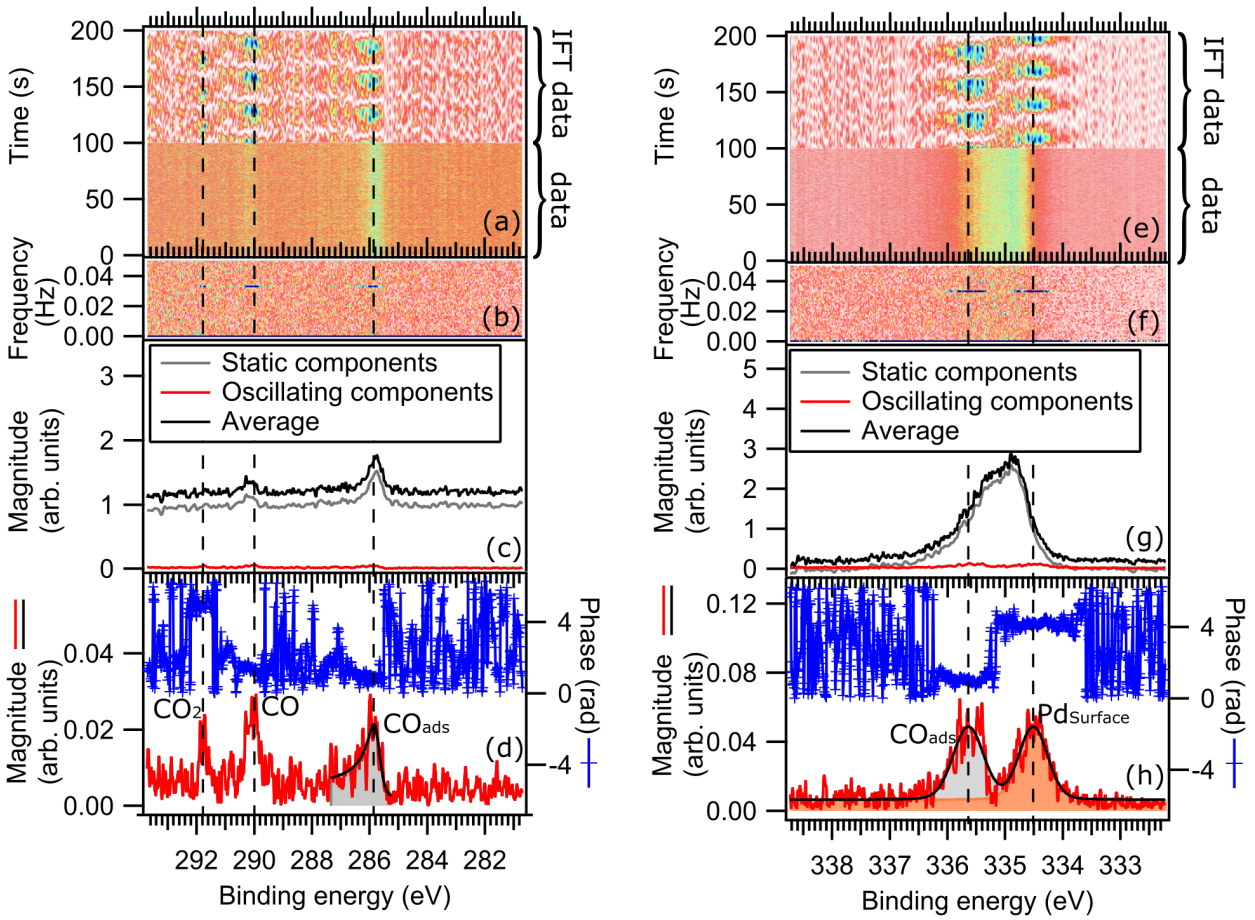

C 1s surface **Pd $3d_{5/2}$ surface**

Figure 18: **Image plot and Fourier transform of time-resolved C 1s/Pd $3d_{5/2}$ surface spectra**, photon energy 510 eV/450 eV, CO:O_2 of 2:2 sccm, temperature oscillation between T = 233°C and T = 293°C with a period of 30 s, (a) Image plot (top half: IFT image plot (4 harmonics), bottom half: energy and transmission-corrected normalized data) (e) Image plot (top half: IFT image plot (4 harmonics), bottom half: energy and transmission-corrected normalized data with removed background) (b)/(f) Oscillation amplitude as a function of frequency and E_{Bin} (c)/(g) Comparison of the oscillating component, the static components and the time average of the image plot (d)/(h) 0.033 Hz oscillation amplitude and phase spectrum

As also observed for the Pt, the Pd surface spectra have much more background noise than the gas spectra. As explained at the beginning of this section for the Pd spectra the secondary electron background was fitted and subtracted to improve the quality of the results, this was unfortunately not possible for the C 1s surface spectra since the background was too noisy to fit it properly. The bad signal-to-noise ratio is due to the fact that only a very small part of the surface is oscillating as shown in Figure 18 (c) and (g) when comparing the magnitude of the oscillations and the static background.

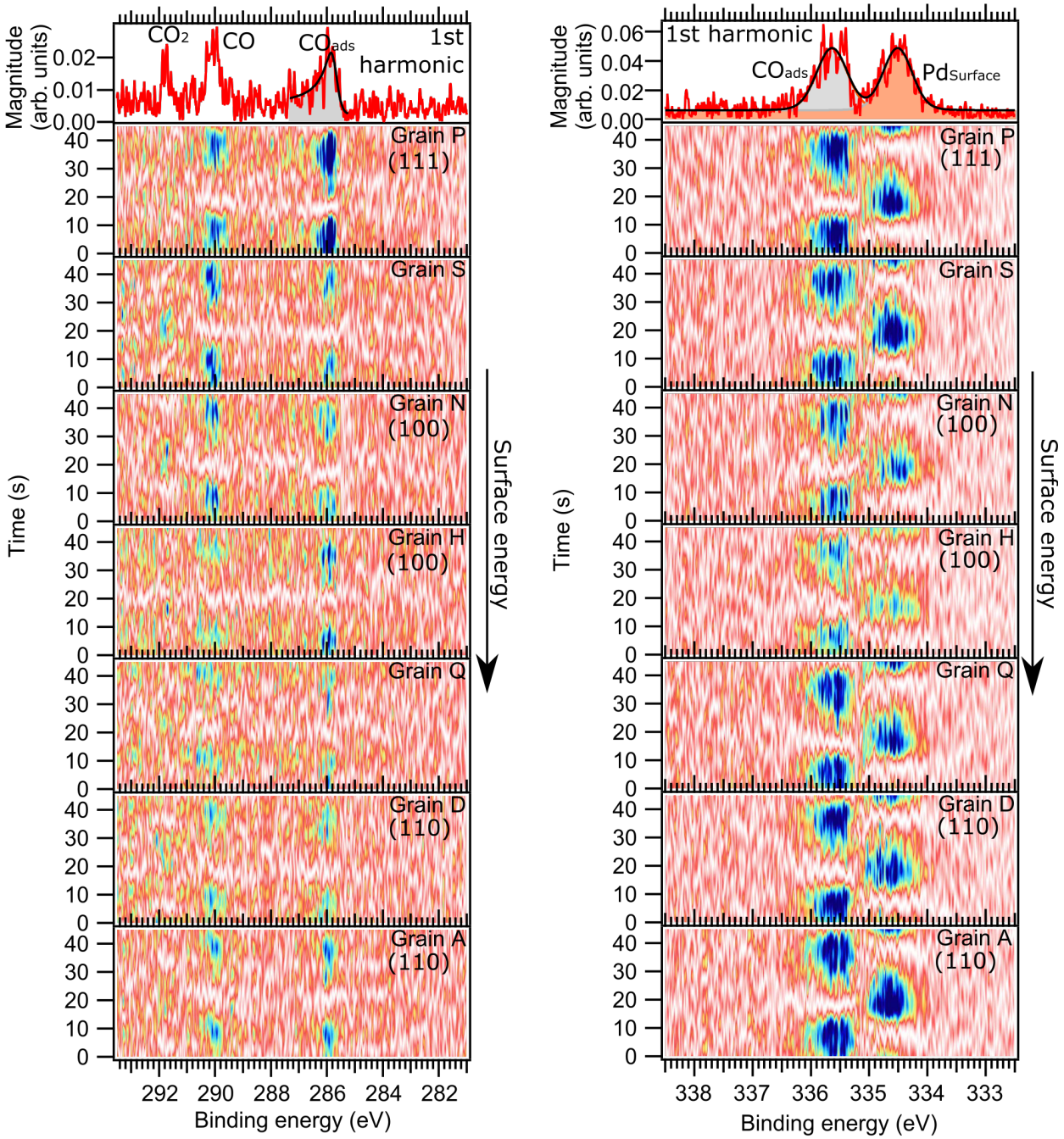

(a) **C 1s surface** (b) **Pd $3d_{5/2}$ surface**

Figure 19: **IFT Image plots (4 harmonics) of C 1s/Pd $3d_{5/2}$ surface spectra for different grains**, photon energy 510 eV/450 eV, CO:O_2 of 2:2 sccm, temperature oscillation between T = 233°C and T = 293°C with a period of 30 s, top panel: 0.033 Hz oscillation amplitude of N grain for peak comparison, other panels: IFT image plots sorted from most closed (top) to most open surface (bottom)

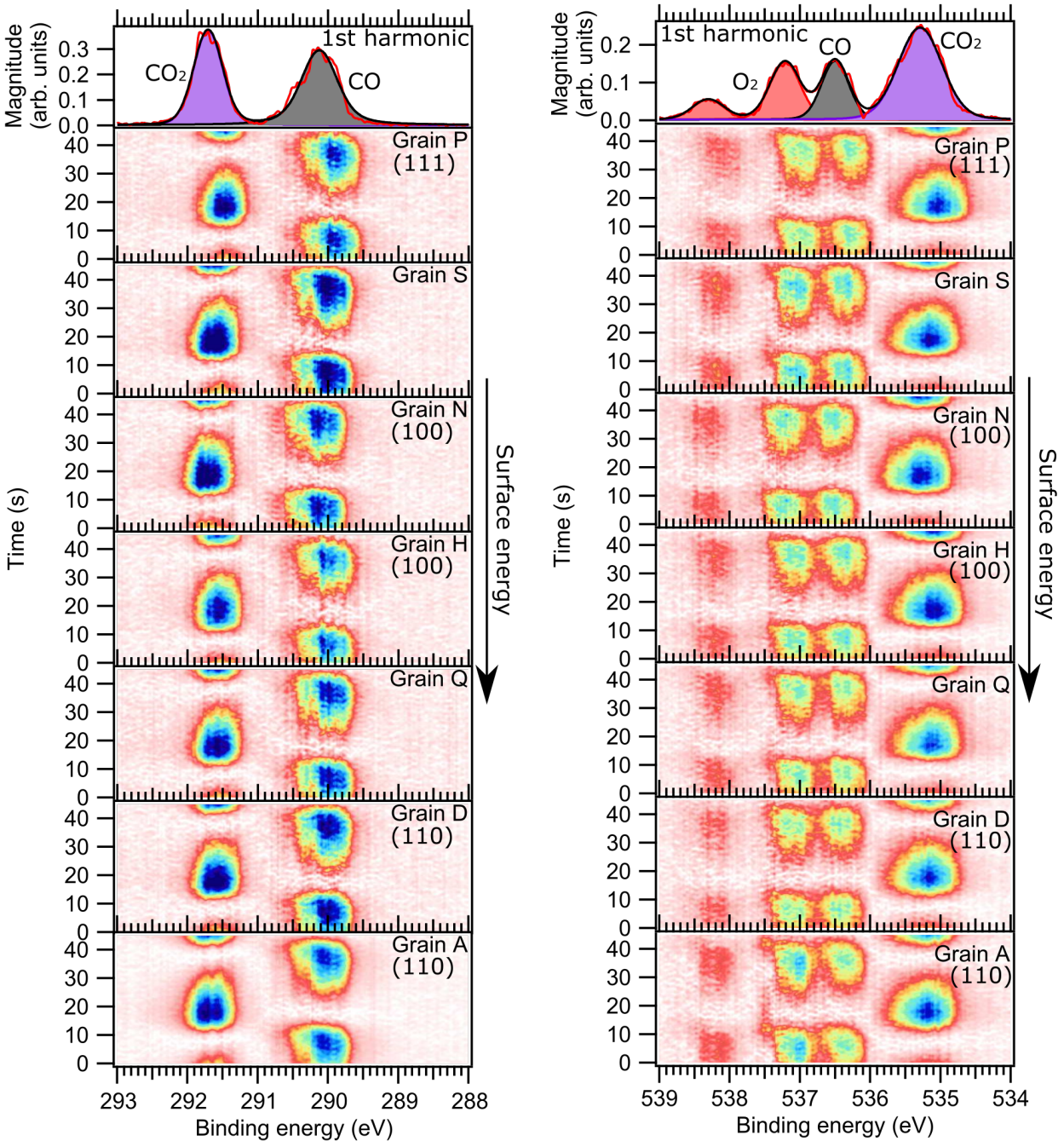

(a) **C 1s gas phase** (b) **O 1s gas phase**

Figure 20: **IFT Image plots (20 harmonics) of C 1s/O 1s gas phase spectra for different grains**, photon energy 510 eV/650 eV, CO:O_2 of 2:2 sccm, temperature oscillation between T = 233°C and T = 293°C with a period of 30 s, top panel: 0.033 Hz oscillation amplitude of N grain for peak comparison, other panels: IFT image plots sorted from most closed (top) to most open surface (bottom)

The static components (grey) in Figure 18 (c) as well as the image plot of the C 1s surface spectra (see Figure 18 (a)) clearly show that there is a strong peak at 285.9 eV,

which corresponds to CO adsorbed to the Pd surface. This means that most of the catalyst surface is covered with CO at all times. The 0.033 Hz components also show the peak from CO adsorbed to the surface, but with much lower intensity, see Figure 18 (d). This means that there is a small part of the surface/vacancies on the surface that are oscillating between being CO-covered and not. The spectrum shows one further peak at around 290 eV which was already previously identified as CO in the gas phase. Taking a closer look at the phase values a third peak can be found at 291.9 eV, which corresponds to CO_2 in the gas phase. As observed before the CO and CO_2 peaks have a phase shift of approximately π to each other. The phase values also depict that the CO peak in the gas phase and CO adsorbed to the surface have the same phase value. Consequently, this implies that when the catalyst is more covered with CO it is less active.

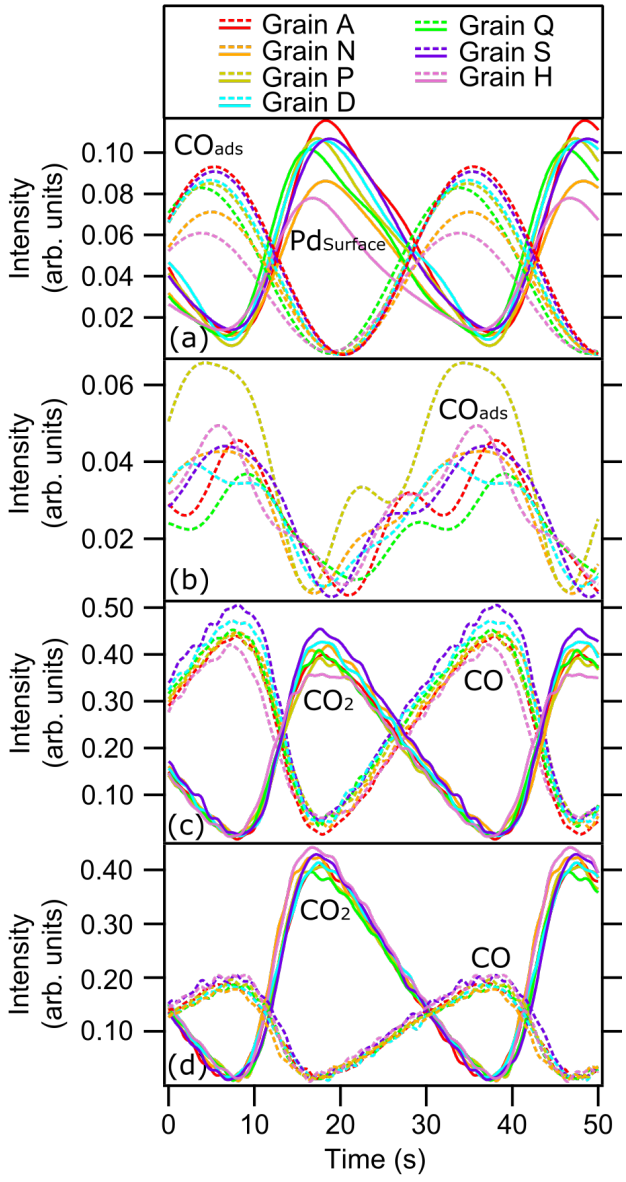

Figure 21: **Vertical integrated intensity of selected peaks** $CO:O_2$ of 2:2 sccm, temperature oscillation between T = 233°C and T = 293°C with a period of 30 s, (a) Pd $3d_{5/2}$ surface (b) C 1s surface (c) C 1s gas phase (d) O 1s gas phase

Further information about the surface coverage can be gained from the Pd surface spectra in Figure 18 (e) to (h). When only looking at the image plot (e) or the static component in (g) only one broad peak can be seen. This peak is caused by an overlapping of two peaks: the bulk component of Pd and CO adsorbed to the surface. But the 0.033 Hz component in Figure 18 (h) clearly shows two peaks: CO adsorbed to the surface at 335.6 eV, which is already observed in the C 1s surface spectra, and the Pd surface at 334.5 eV. The phase values clearly show that the two peaks appear alternating. This, along with the data from the other spectra, indicates that the Pd surface atoms are catalytically active, whereas the Pd surface that is entirely covered with CO is inactive.

To now compare the different grains the IFT image plot is used. To allow for direct comparison of the various grains, the IFT image plots are aligned in time and the intensity of the peaks is depicted using the same color scale. Due to the low signal-to-noise ratio of the surface spectra, only 4 harmonics were used for the surface IFT image plots (Figure 19), while 20 harmonics were used for the gas phase IFT image plots (Figure 20). The IFT image plots of the grains are sorted from top to bottom from the most closed to the most open surface.

Starting with the IFT image plots for the surface spectra it can be seen that all grains are changing from being predominantly CO-covered to having more vacancies of clean Pd. Figure 21 shows the intensity evolution of the different peaks over time. These plots were created by vertically integrating over the peaks in the IFT image plot along the time. The intensity evolution of the measured clean Pd surface is increasing rapidly and then falling slowly for all grains, see Figure 21 (a). This behaviour can also be seen in the temperature pulse (Figure 16 (a)). The fast temperature increase, in the beginning, is due to the exotherm CO oxidation that produces additional heat, causing a faster temperature increase. The matching time evolution of the Pd vacancies and the temperature clearly shows that the surface coverage is strongly dependent on the temperature. The surface coverage is changing gradually, opening up more and more vacancies the higher the temperature gets. The matching intensity evolution of the CO_2 production from the gas phase, see Figure 21 (c) and (d), proves that the clean Pd atoms in the vacancies in the mostly CO-covered catalysts are catalytic active. This can be explained since free Pd atoms are needed for O_2 molecules to dissociate. Hence the more free Pd atoms are available, meaning the more vacancies are formed, the more O_2 can dissociate, and thus the more CO_2 can be produced.

The curve of the adsorbed CO in the $3d_{5/2}$ Pd IFT image plot as well as in the C 1s surface spectra has the inverted curve shape of the Pd surface atoms, see Figure 21 (a) and (b). With the fastly increasing temperature, the CO atoms desorb quickly and then adsorb slowly again on the catalyst when the temperature is decreasing. The oscillating CO components from the gas phase show the same behaviour as expected.

All grains show the same behaviour and dependency on the temperature. Furthermore, the IFT image plots show some indications that the amount of clean palladium atoms depends on the crystallographic orientation. The $3d_{5/2}$ Pd IFT image plots in Figure 19 (b) show that surface coverage oscillates less for the N and H grains in comparison to the other grains. These two grains have an orientation close to (100). Unfortunately, the surface spectra especially the C 1s surface spectra are very noisy making it difficult to find hard evidence for the dependency. Additionally, also the gas phase IFT image plots in Figure 20 do not show any difference between the different grains. Therefore, it would be beneficial to repeat the measurements with larger temperature oscillation while still staying in the CO-poisoned state as well as using a higher frame rate to improve the resolution of the measurement as well as to include the O 1s surface spectra in the analysis.

6.3 Comparison of different grains driving into and out of the mass transfer limit

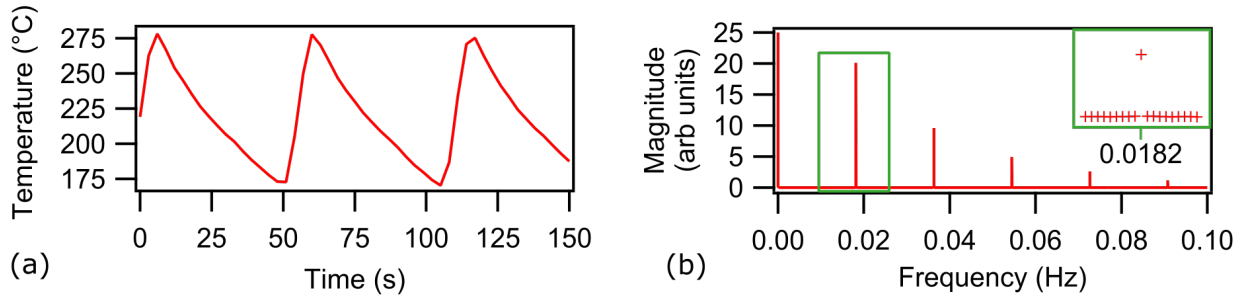

Figure 22: **Temperature oscillations** (a) Temperature data (b) FFT

To reach the CO-MTL the gas composition was changed to 3:1 O_2: CO and larger temperature oscillations between 170 °C and 278 °C with a period of 55 s were used. The resulting driving frequency of $f = \frac{1}{55\ \mathrm{s}} \approx 0.018$ Hz can also be seen in the FT of the temperature data, see Figure 22.

First, the (100) orientated N grain will be discussed in detail, using the knowledge from papers [24, 33, 47] for peak assignments. Afterwards, a comparison will be made with the measurements of the other grains. The following data analysis is done similarly to the previous experiments, including time aligning the different spectra for easier comparison. Since the layout of the figures is identical to the data analysis of the CO-poisoned study, this section will concentrate on the most important details/figures.

The oscillation amplitude of the C 1s gas phase spectrum in Figure 23 (d) shows the same two oscillating peaks as observed in the previous experiment: CO_2 at 291.5 eV and CO at 289.9 eV with a phase shift of approximately π. A closer look at the phase values reveals a small phase shift at 291.1 eV, marked with a green arrow. This component can be identified as -0.4(4) eV work function shifted CO_2. Focusing on the shape of the magnitude of the CO peak reveals two vibrational components of CO, marked with grey arrows, on the left side of the peak. The CO peak in the image plot (a) as well as the static component in (c) also clearly shows that the CO-MTL is reached since all CO is combusted .

The three peaks from the C 1s gas phase spectra can also be identified in the oscillation amplitude of the O 1s gas phase spectrum, see Figure 23 (h). CO is located at 536.3 eV with a phase shift of π relative to the CO_2 peak at 535.1 eV. Similar to the C 1s spectra, only the phase values show the -0.5(4) eV work function shifted CO_2 peak, marked with a green arrow. The CO peak is in phase with the oxygen doublet at 538.0 eV and 536.8 eV. As this experiment is carried out in the CO-MTL, the oxygen is not completely combusted. As a result, two work function shifted O_2 peaks are observed at 538.5 eV (shifted by +0.5(5) eV) and 537.4 eV (shifted by +0.5(1) eV), in phase with the CO_2 peak.

The oscillating and static components for both gas phase spectra in Figures 23 (c) and (g) show that the CO peak is oscillating between no intensity and maximum intensity. This clearly shows that the catalyst is oscillating between a surface that converts all CO to CO_2 (i.e. no CO is observed) and one that only converts CO partly (i.e. CO is observed).

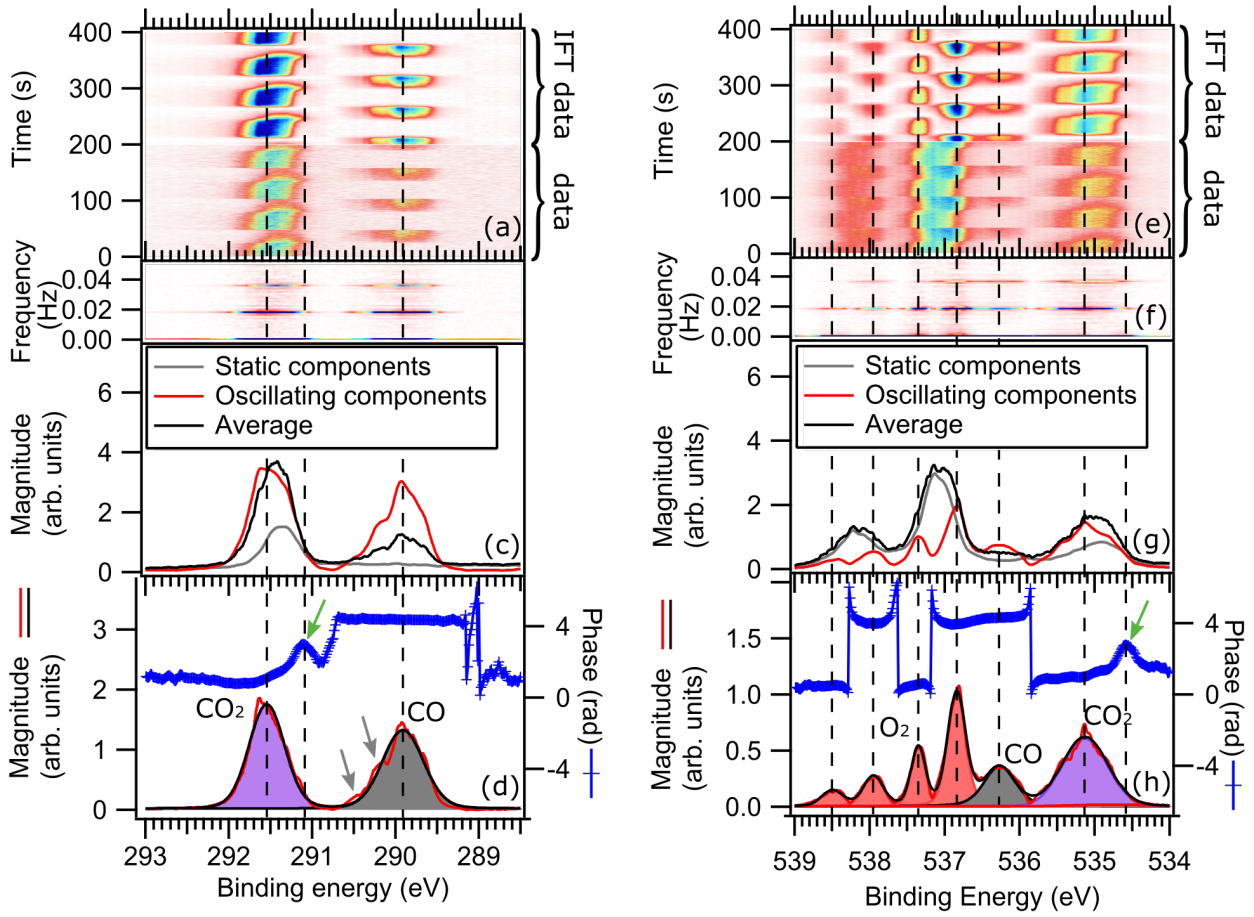

C 1s gas phase **O 1s gas phase**

Figure 23: **Image plot and Fourier transform of time-resolved C 1s/O 1s gas phase spectra**, photon energy 510 eV/650 eV, O_2:CO of 3:1 sccm, temperature oscillation between T = 170°C and T = 278°C with a period of 55 s, (a)/(e) Image plot (top half: IFT image plot (20 harmonics), bottom half: transmission-corrected normalized data) (b)/(f) Oscillation amplitude as a function of frequency and E_{Bin} (c)/(g) Comparison of the oscillating component, the static components and the time average of the image plot (d)/(h) 0.0182 Hz oscillation amplitude and phase spectrum

Figure 24 (d) shows the oscillation amplitude of the C 1s surface spectrum. The left side of the spectrum shows the measured part of the gas phase with the already previously identified peaks. The large additional peak at 285.7 eV can be identified as CO adsorbed (CO_{ads}) to the surface. When looking at the static component at this binding energy in Figure 24 (c) it shows a similar magnitude as the background, proving that the surface

oscillates between being CO-covered and being free of CO. Together with the information from the phase values in Figure 24 (d), which shows that CO_{ads} is in phase with CO in the gas phase, it is evident that CO is only partly combusted when the surface is CO covered.

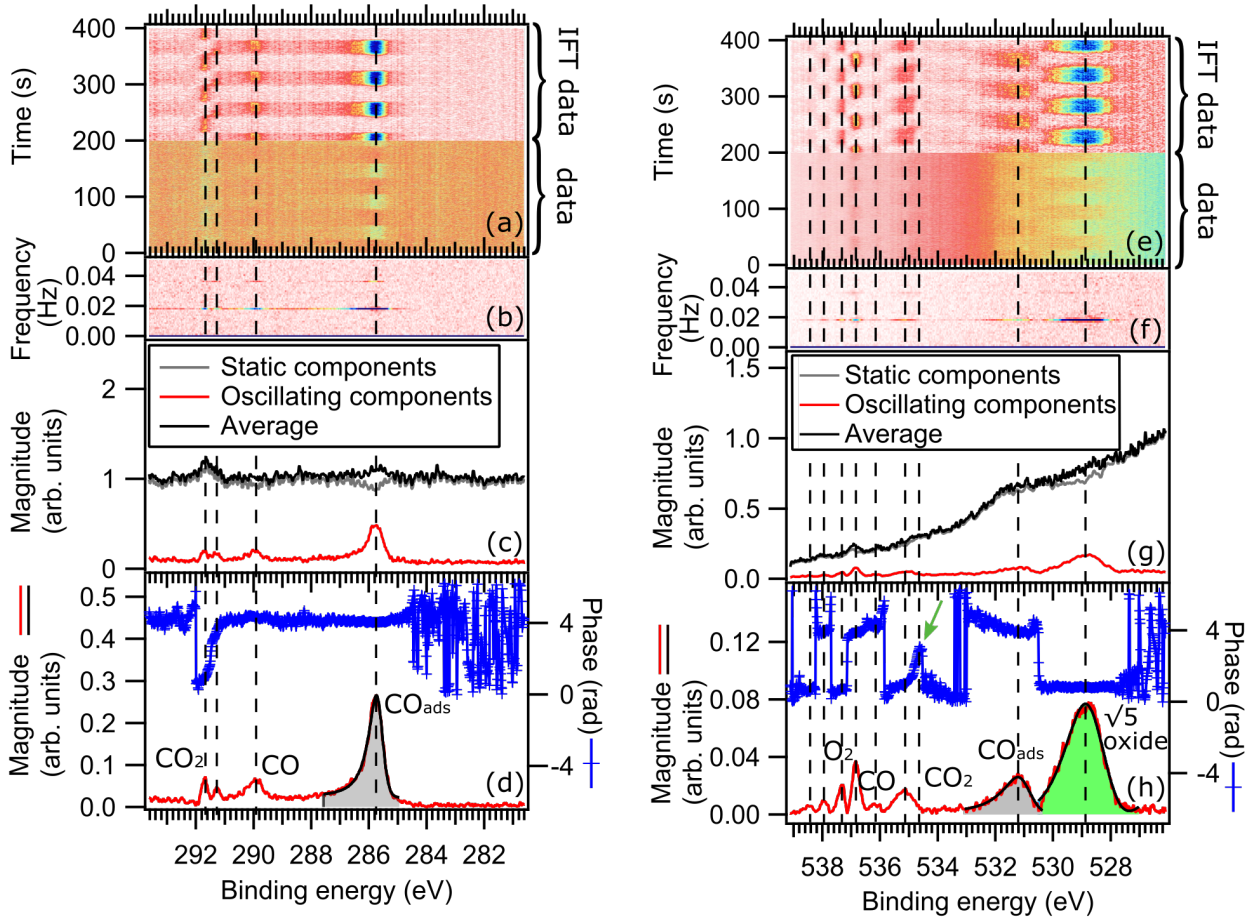

Figure 24: **Image plot and Fourier transform of time-resolved C 1s/O 1s surface spectra**, photon energy 510 eV/650 eV, 3:1 sccm O_2:CO, temperature oscillation between T = 170°C and T = 278°C with a period of 55 s, (a)/(e) Image plot (top half: IFT image plot (20 harmonics), bottom half: energy and transmission-corrected normalized data) (b)/(f) Oscillation amplitude as a function of frequency and E_{Bin} (c)/(g) Comparison of the oscillating component, the static components and the average (offset of +0.2 arb. units) of the image plot (d)/(h) 0.0182 Hz oscillation amplitude and phase spectrum

The O 1s surface oscillation amplitude spectrum, see Figure 24 (h) shows two oscillating surface peaks, the peak at 531.2 eV can be identified as adsorbed CO, while the second observed peak at 528.9 eV is characteristic of $(\sqrt{5} \times \sqrt{5})$R27° oxide (short $\sqrt{5}$ oxide). When observing this oxide two peaks are expected, one at 528.8 eV and one at 529.5 eV, which correspond to surface and interface oxygen atoms in the $(\sqrt{5} \times \sqrt{5})$R27° oxide structure, respectively [33]. Since both expected peaks are relatively close in binding energy, the ob-

served peak could also be a superposition of both peaks.

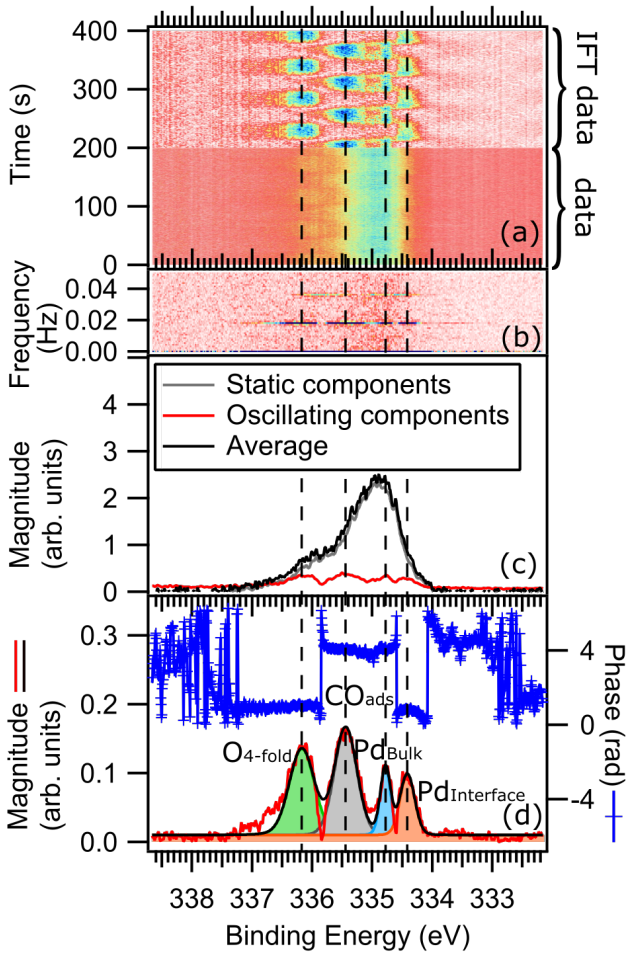

Figure 25: **Image plot and Fourier transform of time-resolved Pd 3d surface**, photon energy 450 eV, 3:1 sccm O_2:CO, temperature oscillation between T = 170°C and T = 278°C with a period of 55 s, (a) Image plot (top half: IFT image plot (20 harmonics), bottom half: energy and transmission-corrected normalized data with removed background) (b) Oscillation amplitude as a function of frequency and E_{Bin} (c) Comparison of the oscillating component, the static components and the time average of the image plot (d) 0.0182 Hz oscillation amplitude and phase spectrum

Additionally, the left side of the spectrum shows peaks from the gas phase. The phase value of the adsorbed CO is in phase with the reactants CO and O_2. The assumed $\sqrt{5}$ oxide peak, which has a phase shift of approximately π to the CO adsorbed peak, however, is in phase with the CO_2 peak and the remaining O_2 in the gas phase. This makes it evident that the Pd polycrystal is O-covered when the catalyst is in the CO-MTL. As previously observed in the gas phase spectra, the phase value reveals a second, -0.5(5) eV work function shifted CO_2 peak (marked with a green arrow), which is not in phase with $\sqrt{5}$ oxide peak nor adsorbed CO. The phase value of the work function shifted CO_2 peak indicates that the peak appears when the surface is changing from O covered to CO covered, meaning when the catalyst is changing from being in the CO-MTL to being CO poisoned. The work function shifted CO_2 could be either caused by CO_2 left in the gas phase, which has not been pumped away yet or there could be vacancies left in the CO-covered surface, which leads to the production of the observed CO_2.

The Pd 3d surface oscillation amplitude spectrum in Figure 25 (d) shows four clear peaks, which can be identified from [33]. From left to right they are Pd atoms 4-fold coordinated to oxygen at 336.2 eV (O_{4-fold}), Pd coordinated to CO at 335.4 eV (CO_{ads}), bulk Pd at 334.8 eV (Pd_{Bulk}). The last peak at 334.4 eV could either be the Pd Interface [33] or clean Pd surface [47] since the binding energy of both peaks is very close. The phase values show that the surface/interface

peak is in phase with the O_{4-fold}, meaning that the peak appears when the surface is covered with oxygen. From this observation, I conclude that the peak is caused by the $Pd_{Interface}$. Furthermore, the phase values clearly show that the Pd interface and the O_{4-fold} are in anti-phase with the adsorbed CO and the bulk component. In comparison with the paper [33] a $\sqrt{5}$ surface oxide is expected when the surface is O covered. For an oscillating coverage of a $\sqrt{5}$ surface oxide oscillating Pd peaks assigned to 4- and 2-fold oxygen coordinated and Pd interface atoms are expected. If CO immediately covers $\sqrt{5}$ oxide-free areas when the coverage decreases in the oscillation cycle, a Pd component assigned to surface Pd atoms bound to CO in anti-phase with $\sqrt{5}$ components should appear. As this CO_{ads} component has a predicted binding energy of 335.5 eV [33] which is very close to the expected binding energy position of 2-fold oxygen coordinated Pd 335.3 eV [33], it is expected to observe only the most intense component, which in this case is the CO_{ads} peak. The oscillating bulk component can most likely be explained by the changing surface coverage. The different attenuation of the oxide and the adsorbed CO influence how much of the bulk is probed. The fact that the adsorbed CO and the bulk component are in phase implies that less of the bulk component is measured when the surface is covered with the $\sqrt{5}$ oxide.

Similar spectra were measured for several different grains. To compare the Pd 3d surface spectra, I first discuss 0.0182 Hz oscillation amplitude and phase spectra (see Figure 26). Additionally, the IFT image plots are used again to look at the time evolution of the peaks (see Figure 27). All spectra/image plots are time aligned and for the IFT image plots the same colour scale is used for the intensity, making it possible to directly compare them. The IFT image plots of the grains are sorted from top to bottom from the most closed to the most open surface.

The N grain was measured two times, once at the beginning of the measurements and once at the end after measuring the other grains. The oscillation amplitude spectra of the N grain in Figure 26 (a) and (b) show the same components, but with slightly different intensities. The exact reason for this is unknown, but it could be due to the surface roughening during the experiment, creating more steps at the surface, or due to silicon segregation towards the surface from the bulk. The same four peaks from the N grain can also be identified in Figure 26 (c) for the H grain, which also has a crystallographic orientation close to (100). The spectra of the H grain show a similar intensity distribution as the initial measurement of the N grain. The main difference is that for the H grain, the surface oxide peak has a slightly larger intensity.

A comparison of the (100) orientated spectra with the other spectra in Figure 26 shows that the interphase peak (coloured orange) can be found in every spectrum at the same binding energy. Additionally, the adsorbed CO peak can be detected in all spectra in anti-phase compared to the Pd interface peak. A closer look at the binding energies however reveals that the adsorbed CO peak has a +0.2 eV binding energy shift in grain P, D, K, and I compared to grain N and H, see table 1. This could be caused by the adsorbed CO adsorbing having a different adsorption structure depending on the crystallographic orientation of the grain.

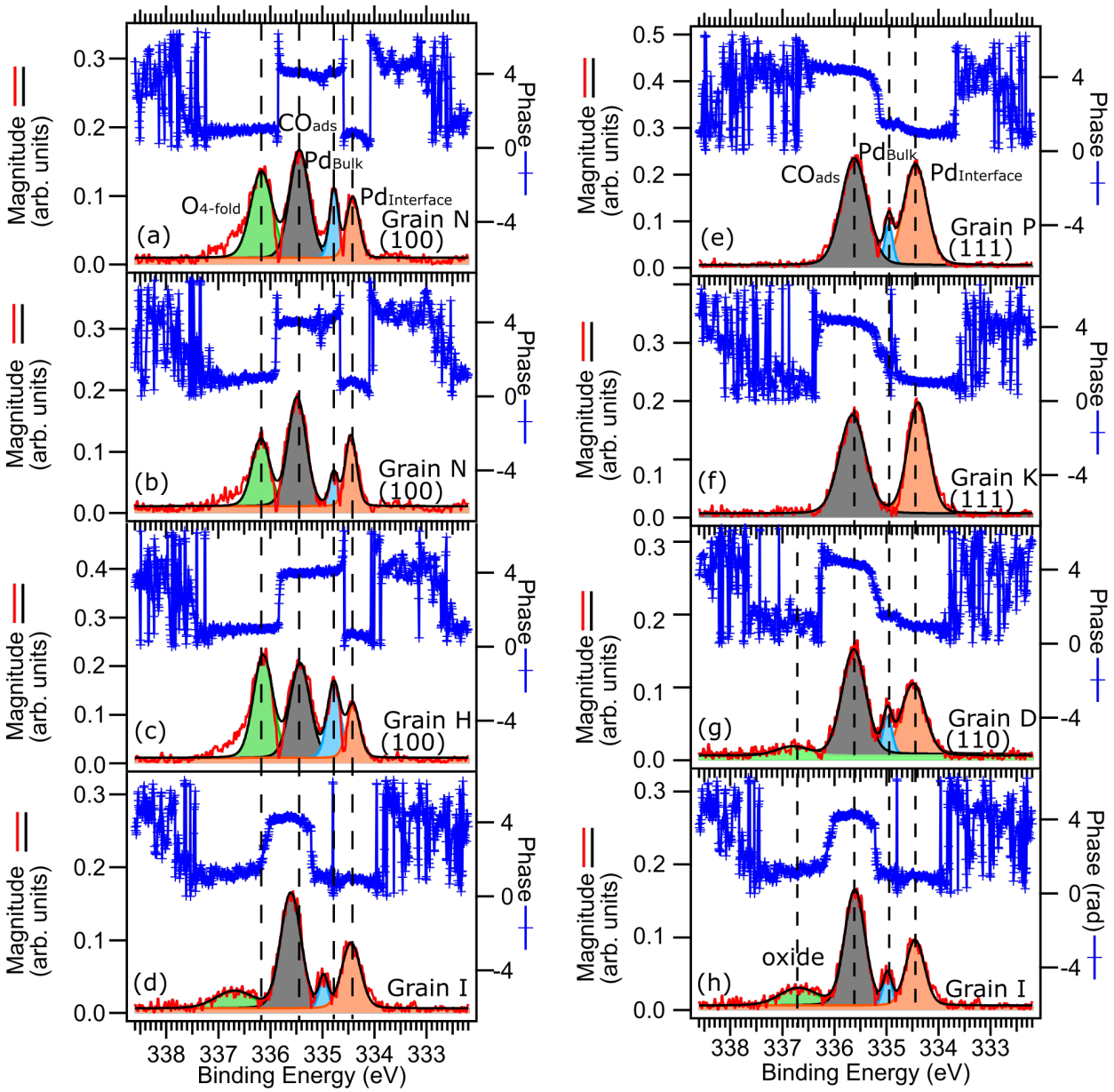

Figure 26: **0.018 Hz oscillation amplitude and phase spectrum of Pd 3d surface for different grains**, photon energy 450 eV, 3:1 sccm O_2:CO, temperature oscillation between T = 170°C and T = 278°C with a period of 55 s, (a) Grain N at beginning of measurements (b) Grain N at end of measurements (c) Grain H (d) Grain I (for comparison of binding energies) (e) Grain P (f) Grain K (g) Grain D (h) Grain I

	Grain N	Grain N	Grain H	Grain P	Grain K	Grain D	Grain I
O_{ads}	336.1(7)	336.1(8)	336.1(4)	-	-	336.8(1)	336.6(9)
CO_{ads}	335.4(4)	335.4(7)	335.4(3)	335.6(2)	335.6(3)	335.6(5)	335.6(1)
Pd_{bulk}	334.7(8)	334.8(0)	334.8(1)	334.9(6)	-	334.9(0)	334,9(8)
$Pd_{surface}$	334.4(1)	334.4(5)	334.4(1)	334.4(4)	334.4(9)	334.3(9)	334.4(5)

Table 1: Binding energies of the Pd 3d surface peaks for the different grains

Another interesting observation is that the bulk component of grains P, D, and I are also shifted by +0.2 eV and is now in phase with the Pd interface, which can also be seen in the IFT image plots in Figure 27. This implies that contrary to the measurements on the (100) surface, for the other crystallographic orientations more of the bulk component is measured when the surface is covered with O. This is hinting that the amount of O atoms adsorbed to the surface is lower compared to the (100) surface. Another possible explanation could be that CO adsorbs in a different adsorption structure, resulting in more CO being adsorbed to the surface in total. A possible explanation for the binding energy shift in the bulk component could be that actually not the bulk component is measured, but rather the second/third layer of the catalyst. These top layers are still influenced by the surface structure/surface coverage due to being the second nearest neighbours to the surface Pd atoms. The K grain is the only grain that does not show the bulk component, which can be seen in Figure 26 (f) as well as in the IFT image plot in Figure 27.

The biggest difference between the spectra is that the O_{4-fold} peak can only be found in the (100) orientated grains. However, the O surface spectra, see Figure 28 (b) show oxygen adsorbed to the surface in all spectra.

In comparison with the paper [32] for Pd(111) orientated grains P and K a $\sqrt{6}$ surface oxide is expected. For this structure two O peaks are expected: one high-intensity peak at 335.5 eV of Pd coordinated to two O molecules and one peak with very low-intensity Pd coordinated to four O molecules at 366.3 eV. As already explained for the Pd(100) surface, the Pd coordinated to two O molecules cannot be observed since the expected peak has nearly the same binding energy as the stronger CO_{ads} peak. The Pd coordinated to 4 O atoms component was not observed in these measurements, which could be due to the resolution since the predicted peak is supposed to have quite low intensity.

The Pd(110) orientated D grain and I grain (orientation between a Pd(111) and a Pd(110)) shows one additional peak at 336.8 eV (336.7 eV respectively). This peak is most likely caused by a surface oxide since the peak is in phase with the Pd interface. Since the component is quite small, especially in the D grain, it is difficult to determine the precise peak position. In reference to [31] a peak corresponding to Pd atoms coordinated to four oxygen atoms is expected to appear at around 336.2 eV, which does not match with the observed peak. The paper [31] observed further peaks caused by surface oxide at 335.4 eV and 335.6 eV, which unfortunately have again nearly the same binding energy as the adsorbed CO [46].

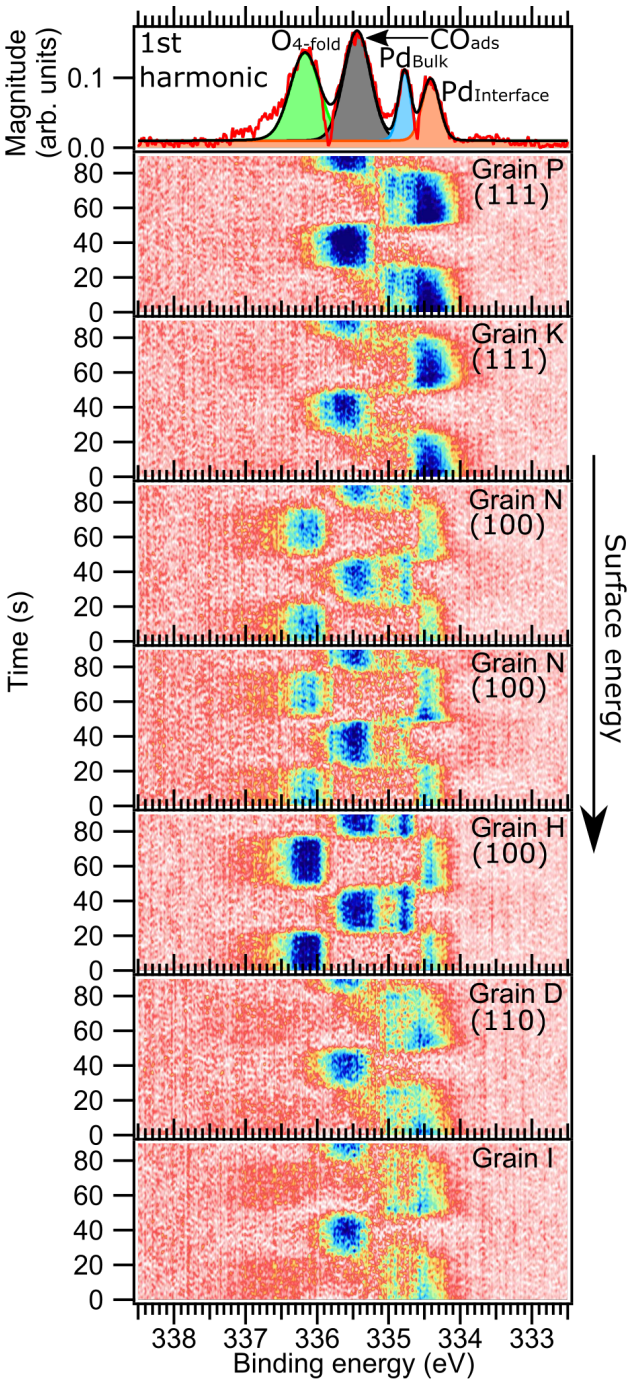

Figure 27: **IFT image plots (20 harmonics) of Pd $3d_{5/2}$ surface**, $h\nu = 450$ eV, same conditions as in Figure 26, top panel: 0.018 Hz oscillation amplitude spectra of N grain for peak comparison, other panels: IFT image plots sorted from most closed (top) to most open surface (bottom)

The good agreement between the Pd spectra of the grains and the literature clearly shows that the measuring setup makes it possible to measure the single grains of the polycrystal individual. This makes it possible to study the oscillating CO/O structures on different grains when the surface is driven into and out of the CO-MTL under the exact same surrounding conditions.

Contrary to the Pd 3d surface (see Figure 27), the O 1s and C 1s surface spectra all show the same components, but with differences in intensity, see Figure 28. Starting with the O 1s surface spectra in Figure 28 (b) a clear dependence can be seen between the intensity of the oscillating surface oxide component and the crystallographic orientation. The intensity shows that more O atoms adsorb and desorb from the surface on the (100) orientated N and H grains than on the other grains. The lowest amount of oxygen adsorb and desorb on the (111) orientated P and K grain. This is also evident from Figure 29 (a), which shows the vertical integration over the single peaks, illustrating the intensity evolution of the peaks in dependence on time. The different amounts of adsorbed/desorbed oxygen are most likely caused by different oxide structures developing on the surface.

Taking a closer look at the IFT image plots of the C 1s surface spectra, see black arrows in Figure 28 (a) clearly show the difference for the P and K grain. While the other grains switch rapidly between CO and O-covered, these two grains change more gradually from oxide-covered to CO-covered.

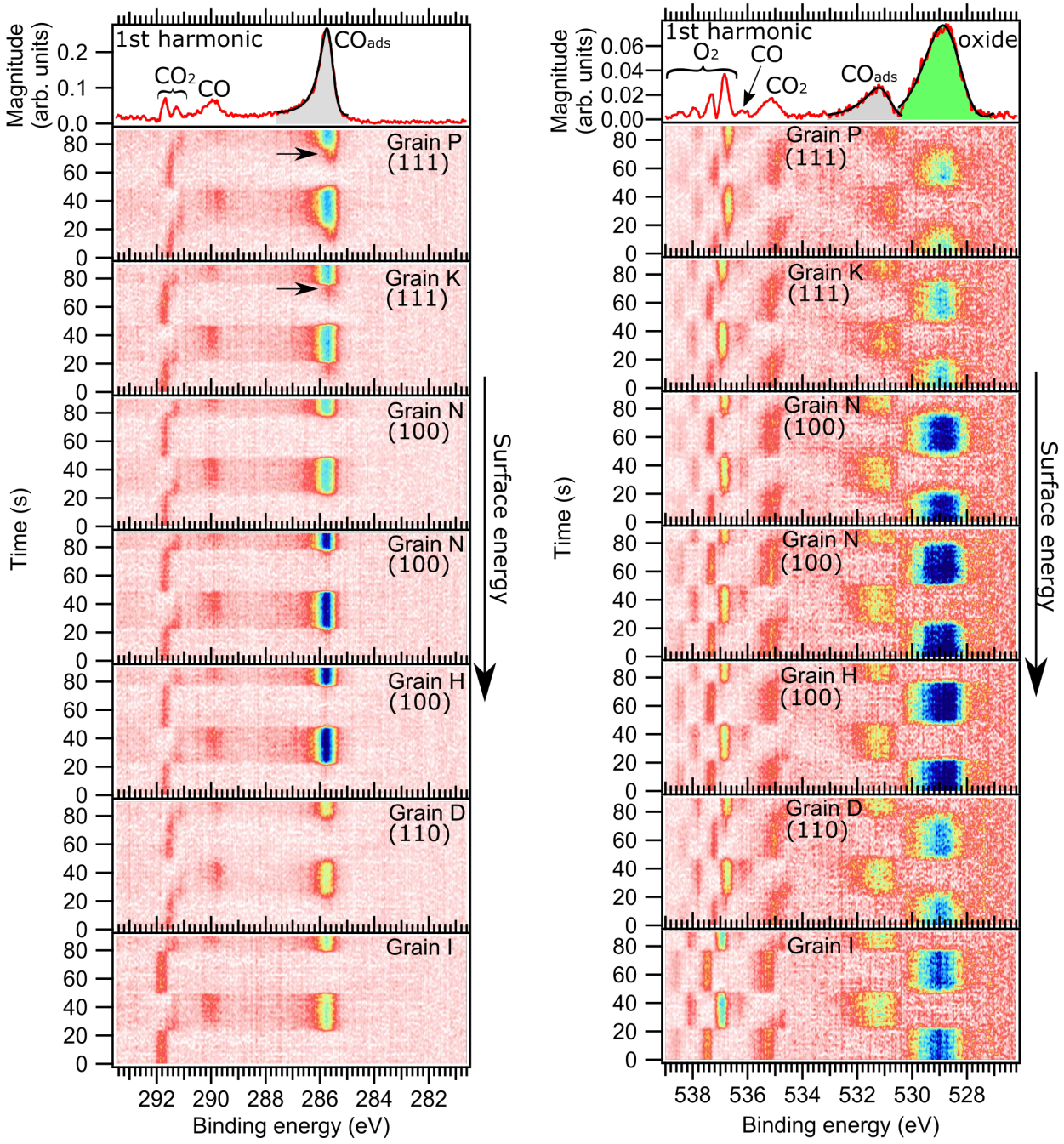

(a) **C 1s surface** (b) **O 1s surface**

Figure 28: **IFT image plots (20 harmonics) of time-resolved C 1s and O 1s surface**, photon energy 510 eV/650 eV, 3:1 sccm O_2:CO, temperature oscillation between T = 170°C and T = 278°C with a period of 55 s, top panel: 0.018 Hz oscillation amplitude of N grain for peak comparison, other panels: IFT image plots sorted from most closed (top) to most open surface (bottom)

The IFT image plot (Figure 28 (a)), as well as the vertical integration over the peaks in Figure 29 (c), show that for the K and P grain CO is adsorbed earlier to the surface. That is

CO starts to adsorb earlier at higher temperatures when the surface temperature is lowered than for the other grains. The vertical integration over the adsorbed CO from the C 1s surface spectra (see Figure 29 (c)) shows that the peak reaches a lower intensity plateau first before rapidly getting completely covered with CO, marked with a green arrow in Figure 29 (c). Unfortunately, this is difficult to see in the vertical integration of the adsorbed CO peak from the O 1s IFT image plot, see Figure 29 (b) due to the lower intensity of the observed peaks and therefore to the higher signal-to-noise ratio.

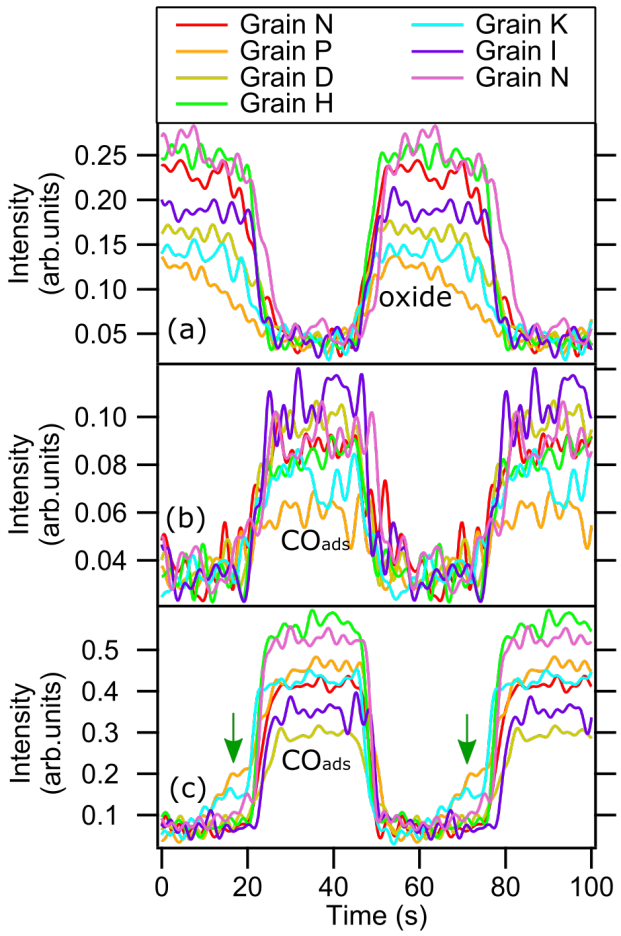

Figure 29: **Vertical integrated intensity of selected peaks** (a) Oxide peak in O 1s surface spectra (b) CO_{ads} peak in O 1s surface spectra (c) CO_{ads} peak in C 1s surface spectra

This different behaviour can also be seen in the O 1s gas phase IFT image plot, see the black dotted box in Figure 30 (b). When comparing the work function shifts of the stronger peak of the O_2 doublet for the different grains it can be seen that for the N grain, it changes rapidly. In comparison the P grain the O_2 peak slowly loses intensity, meanwhile the work function shifted O_2 peak is already appearing and coexisting with the other peak. The coexistence of these two peaks shows that O_2 molecules above an O-covered and a CO-covered surface exist simultaneously. This indicates that on the surface CO-covered "island"/vacancies are developing, while the catalyst is still O-covered. The C 1s surface IFT image plot 28 (a) shows that the amount of adsorbed CO on the surface is happening gradually until a certain plateau is reached (marked with a green arrow in Figure 29 (c)) and then quickly switches to predominantly CO-covered. Further evidence for this comes from the time evolution of the CO_2 peak in the C 1s and O 1s gas phase IFT image plots for the P grain, see Figure 30. They clearly show that the CO_2 peak is gradually slightly shifting in energy, see the green dashed box in Figure 30 (b). This is most likely due to a superposition of the CO_2 and the work function shifted CO_2 peak, which is slowing changing in intensity and so is causing the gradual drift of the superposition. At the "end" of the CO_2 peak, there is a small rapid shift in binding energy (see black arrows in Figure 30 (b)), this is most likely caused by the surface going from having islands of adsorbed CO to being predominantly CO-covered, meaning the second CO_2 component rapidly disappears. This rapid shift in binding energy can also be observed for the N and D grains when the

surface changes rapidly from O to CO-covered.

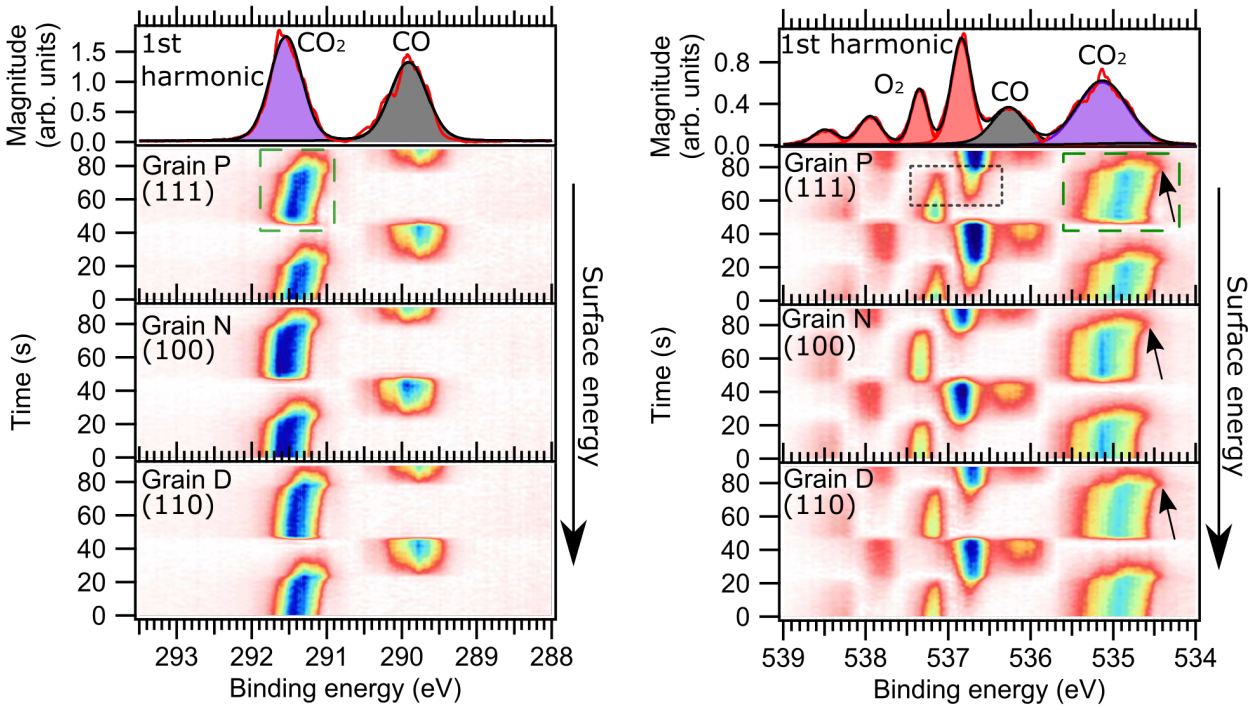

(a) **C 1s gas phase** (b) **O 1s gas phase**

Figure 30: **IFT image plots (20 harmonics) of time-resolved C 1s and O 1s gas phase**, photon energy 510 eV/650 eV, 3:1 sccm O_2:CO, temperature oscillation between T = 170°C and T = 278°C with a period of 55 s, top panel: 0.018 Hz oscillation amplitude of N grain for peak comparison, other panels: IFT image plots sorted from most closed (top) to most open surface (bottom)

It further can be seen in Figures 28 (a) and 29 (c) that there is a big intensity difference between the first and the last measurement of the N-grain in the C 1s surface spectra. This is for unknown reasons. Since this is only the case in the C 1s surface spectra while the O 1s surface spectra for both N grains nearly look identical, I assume that the first measurement of the N grain is an outlier.

These measurements show clearly that it is possible to measure the single grains individually as well as measure the corresponding gas phase for each grain. It also shows that the time-resolved measurement makes it possible to detect that CO is adsorbing differently to the surface depending on the crystallographic orientation of the grain. The fact that CO is adsorbing to the surface at higher temperatures for the (111) like P grain than for the (100) N and (110) D grain, suggests that the (100) and (110) orientations are preferable for industrial use since coverage with CO normally means that the catalyst is getting less active.

7 Conclusion and Outlook

In my thesis, I was able to show that we can navigate on a polycrystal and measure grains individually. It is not only possible to measure the specific surface spectra but also to measure the corresponding gas phase spectra for each grain. The use of Fourier analysis, especially of the inverse Fourier transformations without the 0 Hz component, makes it possible to observe the time evolution of the changing components driven by temperature oscillations.

The data analysis of the Pt(111) crystal, which oscillates into and out of the MTL, clearly shows how powerful the use of the Fourier transformation is for detecting small changing components. The data revealed a transient state of a clean, catalytic active Pt surface between the CO and O-covered surface, which only appears for a short amount of time. The time evolution of the changing components, which is enabled by the use of the inverse Fourier transform without the 0 Hz component, also proves that the clean Pt transition phase appears longer and with a higher intensity when the catalyst is changing from CO to O covered than in the opposite direction.

The same technique was used to study the different grains of a polycrystalline Pd catalyst. The study of the different grains under identical conditions showed that when the catalyst is driven into and out of the mass transfer limit, all grains oscillate between being CO and O-covered. The spectra showed that the different crystallographic orientations form different surface oxides. The spectra also showed some difference in the adsorption of CO. While most grains rapidly changed between CO to O covered, the Pd(111) grain seems to develop small CO domains/islands while the catalyst is still O covered, before switching to a completely CO covered surface. Since the study showed that the Pd(111) grains are more prone to CO poisoning than the other studied grains, different crystallographic orientations like Pd(100) and Pd(110) would be preferable for industrial applications.

The temperature oscillation, while the catalyst stayed CO-poisoned, showed that there is a strong dependency between the temperature and the opening of vacancies on the surface, causing the catalytic activity. This behaviour could be observed in all grains. The data shows weak evidence that there is a dependency between the crystallographic orientation and the total amount of formed vacancies. To prove this, further measurements are needed. To improve the measurement in the CO mass transfer limit, larger temperature oscillations as well as a higher frame rate should be used. This could also make it possible to include the O 1s surface spectra in the data analysis, which was unfortunately not possible in this study since the O 1s surface spectra were too noisy.

The possibility of measuring different crystallographic orientations under the same condition and directly correlating the catalytic activity using the gas phase spectra opens for many further experiments. Instead of oscillating the temperature, also the pressure or gas composition could be changed periodically, giving more insight into the dependency of the catalyst on the surrounding conditions and coming closer to mimicking industrial conditions. As mentioned in the introduction, industrial catalysts typically consist of particles with different facets on a support material. The knowledge gained from studying different

crystallographic orientations under the same conditions can be used to determine which crystallographic orientation would show the best results under industrial conditions.

Additionally, the use of Fourier transformation as well as the knowledge that it is possible to measure the grains individually, could also be applied to other techniques like hard x-ray photoelectron spectroscopy (HAXPES). The use of HAXPES makes it possible to measure deeper layers of the catalyst to see if they are influenced by the change in the surrounding conditions as well. This could, for example, be interesting for methane oxidation, where earlier studies assumed that carbon is segregating in bulk depending on the temperature [48]. Furthermore, it has already been shown that Fourier transformation can also be used to analyse the changes in the valence band using ultraviolet photoelectron spectroscopy (UPS) [49], which now could also be applied to the measurements of the single grains, to get a deeper insight into the electronic structure.

Maybe most importantly the results discussed in this thesis open for studies of more complex reactions on polycrystals like the production of ammonia from N_2 and H_2 or methane steam reforming, which are essential processes for the transition to use H_2 as an environmentally friendly energy storage system. The understanding and continuous improvement of catalysts are crucial, as they are the key to increasing efficiency in industrial processes, reducing emissions as well as enabling new technologies for a more sustainable future.

8 Acknowledgement

I would like to thank my supervisor Jan Knudsen for the help and support during my thesis as well as for giving me the opportunity to participate in multiple beamtimes during the course of the year. I would also like to thank Ulrike Küst for always answering my questions. Last but now least I want to thank my friends and my family for their ongoing support during my studies.

References

[1] Taylor KC Introduction. In: Taylor KC (ed.), *Automobile Catalytic Converters*, pp. 1–1. Springer. (doi:10.1007/978-3-642-69486-8_1).

[2] GmbH KM. Hydrocracking in the oil & gas industry. https://krohne.com/en/industries/oil-gas-industry/refining-oil-gas-industry/hydrocracking-in-the-oil-and-gas-industry. [Online; accessed 2024-04-23].

[3] El-Deeb ZM, Aboutaleb WA, Mohamed RS, Dhmees AS, Ahmed AI Gasoline and diesel-like fuel production via hydrocracking of hydrotreated tire pyrolytic oil over ni-w/MCM-41 derived from blast furnace slag **103**, 84–93. (doi:10.1016/j.joei.2022.05.013).

[4] Duarte FA, Mello PdA, Bizzi CA, Nunes MAG, Moreira EM, Alencar MS, Motta HN, Dressler VL, Flores M Sulfur removal from hydrotreated petroleum fractions

using ultrasound-assisted oxidative desulfurization process **90**, 6, 2158–2164. (doi: 10.1016/j.fuel.2011.01.030).

[5] Humphreys J, Lan R, Tao S Development and recent progress on ammonia synthesis catalysts for haber–bosch process **2**, 1, 2000043. (doi:10.1002/aesr.202000043). _eprint: https://onlinelibrary.wiley.com/doi/pdf/10.1002/aesr.202000043.

[6] Wang S, Lu A, Zhong CJ Hydrogen production from water electrolysis: role of catalysts **8**, 1, 4. (doi:10.1186/s40580-021-00254-x).

[7] Shi Z, Zhang X, Lin X, Liu G, Ling C, Xi S, Chen B, Ge Y, Tan C, Lai Z, *et al.* Phase-dependent growth of pt on MoS2 for highly efficient h2 evolution **621**, 7978, 300–305. (doi:10.1038/s41586-023-06339-3). Publisher: Nature Publishing Group.

[8] Fajrina N, Tahir M A critical review in strategies to improve photocatalytic water splitting towards hydrogen production **44**, 2, 540–577. (doi:10.1016/j.ijhydene.2018.10.200).

[9] Farias CBB, Barreiros RCS, da Silva MF, Casazza AA, Converti A, Sarubbo LA Use of hydrogen as fuel: A trend of the 21st century **15**, 1, 311. (doi:10.3390/en15010311). Number: 1 Publisher: Multidisciplinary Digital Publishing Institute.

[10] Schühle P, Stöber R, Semmel M, Schaadt A, Szolak R, Thill S, Alders M, Hebling C, Wasserscheid P, Salem O Dimethyl ether/CO2 – a hitherto underestimated h2 storage cycle **16**, 7, 3002–3013. (doi:10.1039/D3EE00228D). Publisher: The Royal Society of Chemistry.

[11] Angeli SD, Monteleone G, Giaconia A, Lemonidou AA State-of-the-art catalysts for CH4 steam reforming at low temperature **39**, 5, 1979–1997. (doi:10.1016/j.ijhydene.2013.12.001).

[12] Campanati M, Fornasari G, Vaccari A Fundamentals in the preparation of heterogeneous catalysts **77**, 4, 299–314. (doi:10.1016/S0920-5861(02)00375-9).

[13] Telaar P, Schwiderowski P, Schmidt S, Stürmer S, Muhler M High-pressure CO, h2, CO2 and ethylene pulses applied in the hydrogenation of CO to higher alcohols over a bulk co-cu catalyst **14**, 15, e202200385. (doi:10.1002/cctc.202200385). _eprint: https://onlinelibrary.wiley.com/doi/pdf/10.1002/cctc.202200385.

[14] Karslıoğlu O, Bluhm H Ambient-pressure x-ray photoelectron spectroscopy (APXPS). In: Frenken J, Groot I (eds.), *Operando Research in Heterogeneous Catalysis*, Springer Series in Chemical Physics, pp. 31–57. Springer International Publishing. (doi:10.1007/978-3-319-44439-0_2).

[15] Bowker M The 2007 nobel prize in chemistry for surface chemistry: Understanding nanoscale phenomena at surfaces **1**, 4, 253–257. (doi:10.1021/nn700356g). Publisher: American Chemical Society.

[16] Woodruff DP Low energy electron diffraction. In: *Reference Module in Materials Science and Materials Engineering*. Elsevier. (doi:10.1016/B978-0-12-803581-8.03400-7).

[17] Caulfield L, Sauter E, Idriss H, Wang Y, Wöll C Bridging the pressure and materials gap in heterogeneous catalysis: A combined UHV, in situ, and operando study using infrared spectroscopy **127**, 29, 14023–14029. (doi:10.1021/acs.jpcc.3c03567). Publisher: American Chemical Society.

[18] Beck A, Paunović V, van Bokhoven JA Identifying and avoiding dead ends in the characterization of heterogeneous catalysts at the gas–solid interface **6**, 10, 873–884. (doi:10.1038/s41929-023-01027-x). Publisher: Nature Publishing Group.

[19] Bridging the pressure and material gap in heterogeneous catalysis **9**, 27, 3459–3459. (doi:10.1039/B706675A). Publisher: The Royal Society of Chemistry.

[20] Zhong L, Chen D, Zafeiratos S A mini review of in situ near-ambient pressure XPS studies on non-noble, late transition metal catalysts **9**, 15, 3851–3867. (doi:10.1039/C9CY00632J). Publisher: The Royal Society of Chemistry.

[21] Somorjai GA, Park JY Concepts, instruments, and model systems that enabled the rapid evolution of surface science **603**, 10, 1293–1300. (doi:10.1016/j.susc.2008.08.030).

[22] Pfaff S, Larsson A, Orlov D, Harlow GS, Abbondanza G, Linpé W, Rämisch L, Gericke SM, Zetterberg J, Lundgren E Operando reflectance microscopy on polycrystalline surfaces in thermal catalysis, electrocatalysis, and corrosion **13**, 16, 19530–19540. (doi:10.1021/acsami.1c04961). Publisher: American Chemical Society.

[23] Pfaff S, Larsson A, Orlov D, Rämisch L, Gericke SM, Lundgren E, Zetterberg J A polycrystalline pd surface studied by two-dimensional surface optical reflectance during CO oxidation: Bridging the materials gap **16**, 1, 444–453. (doi:10.1021/acsami.3c11341). Publisher: American Chemical Society.

[24] Knudsen J, Gallo T, Boix V, Strømsheim MD, D'Acunto G, Goodwin C, Wallander H, Zhu S, Soldemo M, Lömker P, *et al.* Stroboscopic operando spectroscopy of the dynamics in heterogeneous catalysis by event-averaging **12**, 1, 6117. (doi:10.1038/s41467-021-26372-y). Number: 1 Publisher: Nature Publishing Group.

[25] Paleček D, Tek G, Lan J, Iannuzzi M, Hamm P Characterization of the platinum–hydrogen bond by surface-sensitive time-resolved infrared spectroscopy **9**, 6, 1254–1259. (doi:10.1021/acs.jpclett.8b00310). Publisher: American Chemical Society.

[26] Lyu D, Xu J, Wang Z Time-resolved in situ vibrational spectroscopy for electrocatalysis: challenge and opportunity **11**. (doi:10.3389/fchem.2023.1231886). Publisher: Frontiers.

[27] Roger M, Artiglia L, Boucly A, Buttignol F, Agote-Arán M, Bokhoven JAv, Kröcher O, Ferri D Improving time-resolution and sensitivity of in situ x-ray photoelectron spectroscopy of a powder catalyst by modulated excitation **14**, 27, 7482–7491. (doi:10.1039/D3SC01274C). Publisher: The Royal Society of Chemistry.

[28] Müller P, Hermans I Applications of modulation excitation spectroscopy in heterogeneous catalysis **56**, 5, 1123–1136. (doi:10.1021/acs.iecr.6b04855). Publisher: American Chemical Society.

[29] Knudsen J, Eads C, Klyushin A, Temperton R, Küst U, Boix V, Kraina A, Scardamaglia M, Shavorskiy A, Kokkonen E, *et al.* Catalysis in frequency space: Resolving hidden surface structure and activity oscillations. (doi:10.21203/rs.3.rs-4242040/v1). ISSN: 2693-5015.

[30] Pfaff S On the chemical romance between gas and surface, and how to illuminate it .

[31] Westerström R, Weststrate CJ, Resta A, Mikkelsen A, Schnadt J, Andersen JN, Lundgren E, Schmid M, Seriani N, Harl J, *et al.* Stressing pd atoms: Initial oxidation of the pd(1 1 0) surface **602**, 14, 2440–2447. (doi:10.1016/j.susc.2008.05.033).

[32] Martin NM, Van den Bossche M, Grönbeck H, Hakanoglu C, Zhang F, Li T, Gustafson J, Weaver JF, Lundgren E CO adsorption on clean and oxidized pd(111) **118**, 2, 1118–1128. (doi:10.1021/jp410895c). Publisher: American Chemical Society.

[33] Fernandes VR, Bossche MVd, Knudsen J, Farstad MH, Gustafson J, Venvik HJ, Grönbeck H, Borg A Reversed hysteresis during CO oxidation over pd75ag25(100) **6**, 7, 4154–4161. (doi:10.1021/acscatal.6b00658). Publisher: American Chemical Society.

[34] 14.4: Heterogeneous catalysts. `https://chem.libretexts.org/Bookshelves/Inorganic_Chemistry/Inorganic_Chemistry_(LibreTexts)/14%3A_Organometallic_Reactions_and_Catalysis/14.04%3A_Heterogeneous_Catalysts`. [Online; accessed 2024-05-03].

[35] Chemisorption. `https://www.chemie.de/lexikon/Chemisorption.html`. [Online; accessed 2024-04-12].

[36] Langmuir-hinshelwood mechanism - an overview | ScienceDirect topics. `https://www.sciencedirect.com/topics/engineering/langmuir-hinshelwood-mechanism`. [Online; accessed 2024-04-28].

[37] Morad M. Development of new highly active nano gold catalysts for selective oxidation reactions.

[38] Boix V. Graphene: Applications in surface science studies. ISBN: 9789180394475 9789180394482.

[39] Cross-section - online dictionary of crystallography. https://dictionary.iucr.org/Cross-section. [Online; accessed 2024-04-28].

[40] 2.0: Polar covalent bonds - electronegativity. `https://chem.libretexts.org/Bookshelves/Organic_Chemistry/Organic_Chemistry_(Morsch_et_al.)/02%3A_Polar_Covalent_Bonds_Acids_and_Bases/2.00%3A_Polar_Covalent_Bonds_-_Electronegativity`. [Online; accessed 2024-04-22].

[41] Knudsen J, Andersen JN, Schnadt J A versatile instrument for ambient pressure x-ray photoelectron spectroscopy: The lund cell approach **646**, 160–169. (doi:10.1016/j.susc.2015.10.038).

[42] Zhu S, Scardamaglia M, Kundsen J, Sankari R, Tarawneh H, Temperton R, Pickworth L, Cavalca F, Wang C, Tissot H, *et al.* HIPPIE: a new platform for ambient-pressure x-ray photoelectron spectroscopy at the MAX IV laboratory **28**, 2, 624–636. (doi:10.1107/S160057752100103X). Publisher: International Union of Crystallography.

[43] Johansson N. Synchrotron-based in situ electron spectroscopy applied to oxide formation and catalysis. ISBN: 9789177534389 9789177534372.

[44] Björneholm O, Nilsson A, Tillborg H, Bennich P, Sandell A, Hernnäs B, Puglia C, Mårtensson N Overlayer structure from adsorbate and substrate core level binding energy shifts: CO, CCH3 and o on pt(111) **315**, 1, L983–L989. (doi:10.1016/0039-6028(94)90530-4).

[45] Johansson N, Andersen M, Monya Y, Andersen JN, Kondoh H, Schnadt J, Knudsen J Ambient pressure phase transitions over ir(1 1 1): at the onset of CO oxidation **29**, 44, 444002. (doi:10.1088/1361-648X/aa8a44).

[46] Koitaya T, Ishikawa A, Yoshimoto S, Yoshinobu J C–h bond activation of methane through electronic interaction with pd(110) **125**, 2, 1368–1377. (doi:10.1021/acs.jpcc.0c09537). Publisher: American Chemical Society.

[47] Walle LE, Grönbeck H, Fernandes VR, Blomberg S, Farstad MH, Schulte K, Gustafson J, Andersen JN, Lundgren E, Borg A Surface composition of clean and oxidized pd75ag25(100) from photoelectron spectroscopy and density functional theory calculations **606**, 23, 1777–1782. (doi:10.1016/j.susc.2012.07.006).

[48] Küst U Linking the selectivity of varying surface phases of a real palladium catalyst toward specific methane oxidation pathways with ambient pressure x-ray photoelectron spectroscopy .

[49] Ratiu GL Application of fourier transforms to time-resolved ambient pressure spectroscopy operando studies of CO oxidation over pt(111) .